

Sixth Edition

Numerical Methods for Engineers

Steven C. Chapra
Raymond P. Canale

Numerical Methods for Engineers

SIXTH EDITION

Steven C. Chapra

Berger Chair in Computing and Engineering
Tufts University

Raymond P. Canale

Professor Emeritus of Civil Engineering
University of Michigan



Higher Education

Boston Burr Ridge, IL Dubuque, IA New York San Francisco St. Louis
Bangkok Bogotá Caracas Kuala Lumpur Lisbon London Madrid Mexico City
Milan Montreal New Delhi Santiago Seoul Singapore Sydney Taipei Toronto



NUMERICAL METHODS FOR ENGINEERS, SIXTH EDITION

Published by McGraw-Hill, a business unit of The McGraw-Hill Companies, Inc., 1221 Avenue of the Americas, New York, NY 10020.
Copyright © 2010 by The McGraw-Hill Companies, Inc. All rights reserved. Previous editions © 2006, 2002, and 1998. No part of this publication may be reproduced or distributed in any form or by any means, or stored in a database or retrieval system, without the prior written consent of The McGraw-Hill Companies, Inc., including, but not limited to, in any network or other electronic storage or transmission, or broadcast for distance learning.

Some ancillaries, including electronic and print components, may not be available to customers outside the United States.

This book is printed on acid-free paper.

1 2 3 4 5 6 7 8 9 0 VNH/VNH 0 9

ISBN 978-0-07-340106-5

MHID 0-07-340106-4

Global Publisher: *Raghethaman Srinivasan*

Sponsoring Editor: *Debra B. Hash*

Director of Development: *Kristine Tibbetts*

Developmental Editor: *Lorraine K. Buczek*

Senior Marketing Manager: *Curt Reynolds*

Project Manager: *Joyce Watters*

Lead Production Supervisor: *Sandy Ludovissy*

Associate Design Coordinator: *Brenda A. Rolwes*

Cover Designer: *Studio Montage, St. Louis, Missouri*

(USE) Cover Image: © *BrandX/JupiterImages*

Compositor: *Macmillan Publishing Solutions*

Typeface: *10/12 Times Roman*

Printer: *R. R. Donnelley Jefferson City, MO*

All credits appearing on page or at the end of the book are considered to be an extension of the copyright page.

MATLAB™ is a registered trademark of The MathWorks, Inc.

Library of Congress Cataloging-in-Publication Data

Chapra, Steven C.

Numerical methods for engineers / Steven C. Chapra, Raymond P. Canale. — 6th ed.

p. cm.

Includes bibliographical references and index.

ISBN 978-0-07-340106-5 — ISBN 0-07-340106-4 (hard copy : alk. paper)

1. Engineering mathematics—Data processing. 2. Numerical calculations—Data processing. 3. Microcomputers—Programming. I. Canale, Raymond P. II. Title.

TA345.C47 2010

518.02462—dc22

2008054296

PARTIAL DIFFERENTIAL EQUATIONS

PT8.1 MOTIVATION

Given a function u that depends on both x and y , the partial derivative of u with respect to x at an arbitrary point (x, y) is defined as

$$\frac{\partial u}{\partial x} = \lim_{\Delta x \rightarrow 0} \frac{u(x + \Delta x, y) - u(x, y)}{\Delta x} \quad (\text{PT8.1})$$

Similarly, the partial derivative with respect to y is defined as

$$\frac{\partial u}{\partial y} = \lim_{\Delta y \rightarrow 0} \frac{u(x, y + \Delta y) - u(x, y)}{\Delta y} \quad (\text{PT8.2})$$

An equation involving partial derivatives of an unknown function of two or more independent variables is called a *partial differential equation*, or *PDE*. For example,

$$\frac{\partial^2 u}{\partial x^2} + 2xy \frac{\partial^2 u}{\partial y^2} + u = 1 \quad (\text{PT8.3})$$

$$\frac{\partial^3 u}{\partial x^2 \partial y} + x \frac{\partial^2 u}{\partial y^2} + 8u = 5y \quad (\text{PT8.4})$$

$$\left(\frac{\partial^2 u}{\partial x^2} \right)^3 + 6 \frac{\partial^3 u}{\partial x \partial y^2} = x \quad (\text{PT8.5})$$

$$\frac{\partial^2 u}{\partial x^2} + xu \frac{\partial u}{\partial y} = x \quad (\text{PT8.6})$$

The *order* of a PDE is that of the highest-order partial derivative appearing in the equation. For example, Eqs. (PT8.3) and (PT8.4) are second- and third-order, respectively.

A partial differential equation is said to be *linear* if it is linear in the unknown function and all its derivatives, with coefficients depending only on the independent variables. For example, Eqs. (PT8.3) and (PT8.4) are linear, whereas Eqs. (PT8.5) and (PT8.6) are not.

Because of their widespread application in engineering, our treatment of PDEs will focus on linear, second-order equations. For two independent variables, such equations can be expressed in the following general form:

$$A \frac{\partial^2 u}{\partial x^2} + B \frac{\partial^2 u}{\partial x \partial y} + C \frac{\partial^2 u}{\partial y^2} + D = 0 \quad (\text{PT8.7})$$

where A, B , and C are functions of x and y and D is a function of $x, y, u, \partial u / \partial x$, and $\partial u / \partial y$. Depending on the values of the coefficients of the second-derivative terms— A, B, C —

TABLE PT8.1 Categories into which linear, second-order partial differential equations in two variables can be classified.

$B^2 - 4AC$	Category	Example
< 0	Elliptic	Laplace equation (steady state with two spatial dimensions) $\frac{\partial^2 T}{\partial x^2} + \frac{\partial^2 T}{\partial y^2} = 0$
$= 0$	Parabolic	Heat conduction equation (time variable with one spatial dimension) $\frac{\partial T}{\partial t} = k' \frac{\partial^2 T}{\partial x^2}$
> 0	Hyperbolic	Wave equation (time variable with one spatial dimension) $\frac{\partial^2 y}{\partial x^2} = \frac{1}{c^2} \frac{\partial^2 y}{\partial t^2}$

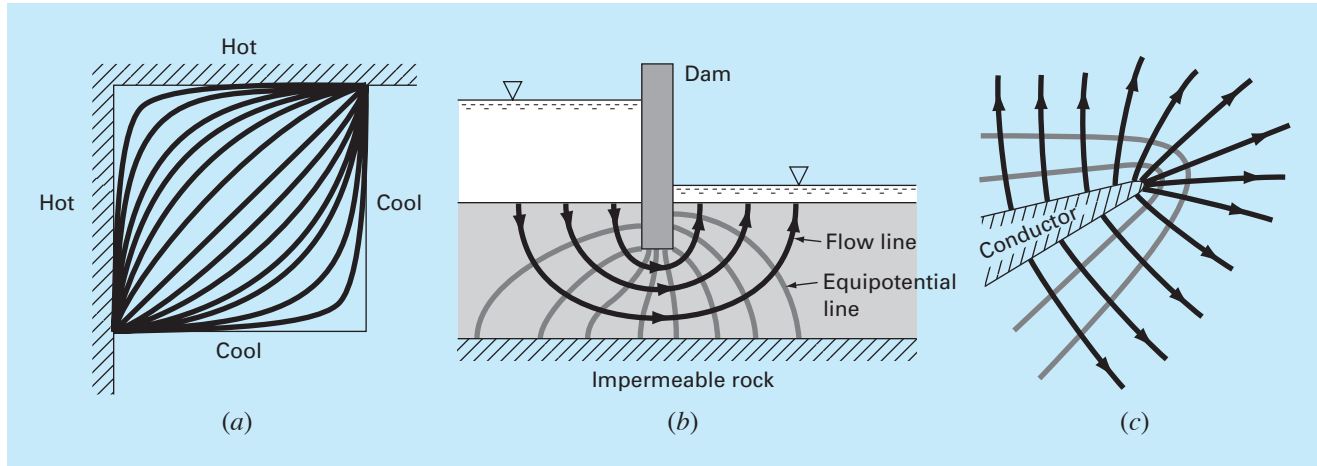
Eq. (PT8.7) can be classified into one of three categories (Table PT8.1). This classification, which is based on the method of characteristics (for example, see Vichnevetsky, 1981, or Lapidus and Pinder, 1981), is useful because each category relates to specific and distinct engineering problem contexts that demand special solution techniques. It should be noted that for cases where A , B , and C depend on x and y , the equation may actually fall into a different category, depending on the location in the domain for which the equation holds. For simplicity, we will limit the present discussion to PDEs that remain exclusively in one of the categories.

PT8.1.1 PDEs and Engineering Practice

Each of the categories of partial differential equations in Table PT8.1 conforms to specific kinds of engineering problems. The initial sections of the following chapters will be devoted to deriving each type of equation for a particular engineering problem context. For the time being, we will discuss their general properties and applications and show how they can be employed in different physical contexts.

Elliptic equations are typically used to characterize *steady-state* systems. As in the *Laplace equation* in Table PT8.1, this is indicated by the absence of a time derivative. Thus, these equations are typically employed to determine the steady-state distribution of an unknown in two spatial dimensions.

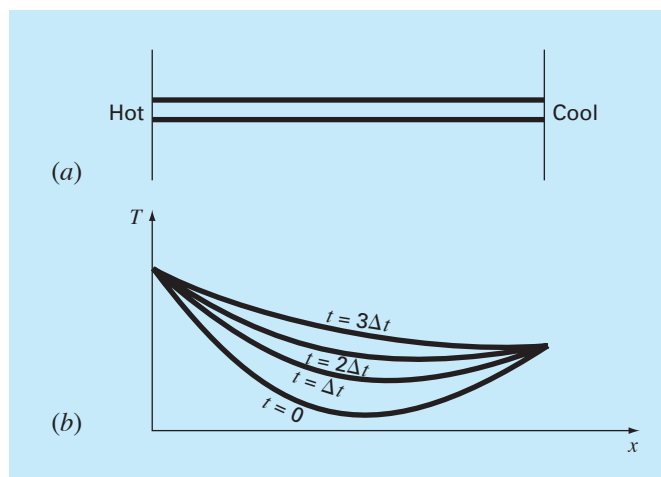
A simple example is the heated plate in Fig. PT8.1a. For this case, the boundaries of the plate are held at different temperatures. Because heat flows from regions of high to low temperature, the boundary conditions set up a potential that leads to heat flow from the hot to the cool boundaries. If sufficient time elapses, such a system will eventually reach the stable or steady-state distribution of temperature depicted in Fig. PT8.1a. The Laplace equation, along with appropriate boundary conditions, provides a means to determine this distribution. By analogy, the same approach can be employed to tackle other problems involving potentials, such as seepage of water under a dam (Fig. PT8.1b) or the distribution of an electric field (Fig. PT8.1c).

**FIGURE PT8.1**

Three steady-state distribution problems that can be characterized by elliptic PDEs. (a) Temperature distribution on a heated plate, (b) seepage of water under a dam, and (c) the electric field near the point of a conductor.

FIGURE PT8.2

(a) A long, thin rod that is insulated everywhere but at its end. The dynamics of the one-dimensional distribution of temperature along the rod's length can be described by a parabolic PDE. (b) The solution, consisting of distributions corresponding to the state of the rod at various times.

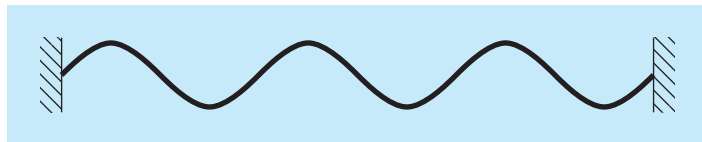


In contrast to the elliptic category, *parabolic equations* determine how an unknown varies in both space and time. This is manifested by the presence of both spatial and temporal derivatives in the *heat conduction equation* from Table PT8.1. Such cases are referred to as *propagation problems* because the solution “propagates,” or changes, in time.

A simple example is a long, thin rod that is insulated everywhere except at its end (Fig. PT8.2a). The insulation is employed to avoid complications due to heat loss along the

FIGURE PT8.3

A taut string vibrating at a low amplitude is a simple physical system that can be characterized by a hyperbolic PDE.



rod's length. As was the case for the heated plate in Fig. PT8.1a, the ends of the rod are set at fixed temperatures. However, in contrast to Fig. PT8.1a, the rod's thinness allows us to assume that heat is distributed evenly over its cross section—that is, laterally. Consequently, lateral heat flow is not an issue, and the problem reduces to studying the conduction of heat along the rod's longitudinal axis. Rather than focusing on the steady-state distribution in two spatial dimensions, the problem shifts to determining how the one-dimensional spatial distribution changes as a function of time (Fig. PT8.2b). Thus, the solution consists of a series of spatial distributions corresponding to the state of the rod at various times. Using an analogy from photography, the elliptic case yields a portrait of a system's stable state, whereas the parabolic case provides a motion picture of how it changes from one state to another. As with the other types of PDEs described herein, parabolic equations can be used to characterize a wide variety of other engineering problem contexts by analogy.

The final class of PDEs, the *hyperbolic* category, also deals with *propagation problems*. However, an important distinction manifested by the wave equation in Table PT8.1 is that the unknown is characterized by a second derivative with respect to time. As a consequence, the solution oscillates.

The vibrating string in Fig. PT8.3 is a simple physical model that can be described with the wave equation. The solution consists of a number of characteristic states with which the string oscillates. A variety of engineering systems such as vibrations of rods and beams, motion of fluid waves, and transmission of sound and electrical signals can be characterized by this model.

PT8.1.2 Precomputer Methods for Solving PDEs

Prior to the advent of digital computers, engineers relied on analytical or exact solutions of partial differential equations. Aside from the simplest cases, these solutions often required a great deal of effort and mathematical sophistication. In addition, many physical systems could not be solved directly but had to be simplified using linearizations, simple geometric representations, and other idealizations. Although these solutions are elegant and yield insight, they are limited with respect to how faithfully they represent real systems—especially those that are highly nonlinear and irregularly shaped.

PT8.2 ORIENTATION

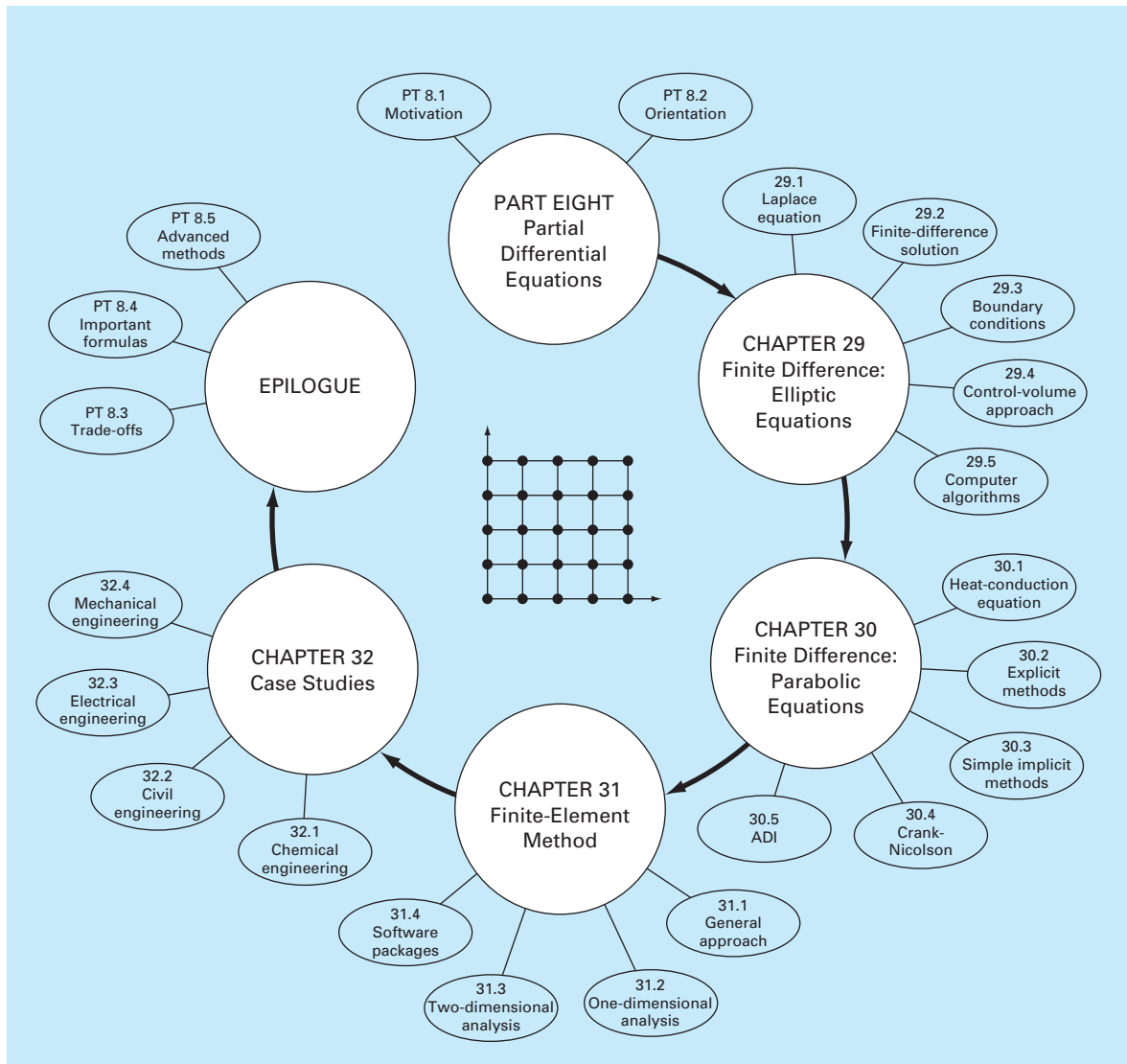
Before we proceed to the numerical methods for solving partial differential equations, some orientation might be helpful. The following material is intended to provide you with an overview of the material discussed in Part Eight. In addition, we have formulated objectives to focus your studies in the subject area.

PT8.2.1 Scope and Preview

Figure PT8.4 provides an overview of Part Eight. Two broad categories of numerical methods will be discussed in this part of this book. Finite-difference approaches, which are covered in Chaps. 29 and 30, are based on approximating the solution at a finite number of points. In contrast, finite-element methods, which are covered in Chap. 31, approximate

FIGURE PT8.4

Schematic representation of the organization of material in Part Eight: Partial Differential Equations.



the solution in pieces, or “elements.” Various parameters are adjusted until these approximations conform to the underlying differential equation in an optimal sense.

Chapter 29 is devoted to *finite-difference* solutions of *elliptic equations*. Before launching into the methods, we derive the Laplace equation for the physical problem context of the temperature distribution for a heated plate. Then, a standard solution approach, the *Liebmann method*, is described. We will illustrate how this approach is used to compute the distribution of the primary scalar variable, temperature, as well as a secondary vector variable, heat flux. The final section of the chapter deals with *boundary conditions*. This material includes procedures to handle different types of conditions as well as irregular boundaries.

In *Chap. 30*, we turn to *finite-difference* solutions of *parabolic equations*. As with the discussion of elliptic equations, we first provide an introduction to a physical problem context, the heat-conduction equation for a one-dimensional rod. Then we introduce both explicit and implicit algorithms for solving this equation. This is followed by an efficient and reliable implicit method—the *Crank-Nicolson technique*. Finally, we describe a particularly effective approach for solving two-dimensional parabolic equations—the *alternating-direction implicit, or ADI, method*.

Note that, because they are somewhat beyond the scope of this book, we have chosen to omit hyperbolic equations. The epilogue of this part of the book contains references related to this type of PDE.

In *Chap. 31*, we turn to the other major approach for solving PDEs—the *finite-element method*. Because it is so fundamentally different from the finite-difference approach, we devote the initial section of the chapter to a general overview. Then we show how the finite-element method is used to compute the steady-state temperature distribution of a heated rod. Finally, we provide an introduction to some of the issues involved in extending such an analysis to two-dimensional problem contexts.

Chapter 32 is devoted to applications from all fields of engineering. Finally, a short review section is included at the end of Part Eight. This epilogue summarizes important information related to PDEs. This material includes a discussion of trade-offs that are relevant to their implementation in engineering practice. The epilogue also includes references for advanced topics.

PT8.2.2 Goals and Objectives

Study Objectives. After completing Part Eight, you should have greatly enhanced your capability to confront and solve partial differential equations. General study goals should include mastering the techniques, having the capability to assess the reliability of the answers, and being able to choose the “best” method (or methods) for any particular problem. In addition to these general objectives, the specific study objectives in Table PT8.2 should be mastered.

Computer Objectives. Computer algorithms can be developed for many of the methods in Part Eight. For example, you may find it instructive to develop a general program to simulate the steady-state distribution of temperature on a heated plate. Further, you might want to develop programs to implement both the simple explicit and the Crank-Nicolson methods for solving parabolic PDEs in one spatial dimension.

TABLE PT8.2 Specific study objectives for Part Eight.

-
1. Recognize the difference between elliptic, parabolic, and hyperbolic PDEs.
 2. Understand the fundamental difference between finite-difference and finite-element approaches.
 3. Recognize that the Liebmann method is equivalent to the Gauss-Seidel approach for solving simultaneous linear algebraic equations.
 4. Know how to determine secondary variables for two-dimensional field problems.
 5. Recognize the distinction between Dirichlet and derivative boundary conditions.
 6. Understand how to use weighting factors to incorporate irregular boundaries into a finite-difference scheme for PDEs.
 7. Understand how to implement the control-volume approach for implementing numerical solutions of PDEs.
 8. Know the difference between convergence and stability of parabolic PDEs.
 9. Understand the difference between explicit and implicit schemes for solving parabolic PDEs.
 10. Recognize how the stability criteria for explicit methods detract from their utility for solving parabolic PDEs.
 11. Know how to interpret computational molecules.
 12. Recognize how the ADI approach achieves high efficiency in solving parabolic equations in two spatial dimensions.
 13. Understand the difference between the direct method and the method of weighted residuals for deriving element equations.
 14. Know how to implement Galerkin's method.
 15. Understand the benefits of integration by parts during the derivation of element equations; in particular, recognize the implications of lowering the highest derivative from a second to a first derivative.
-

Finally, one of your most important goals should be to master several of the general-purpose software packages that are widely available. In particular, you should become adept at using these tools to implement numerical methods for engineering problem solving.

Finite Difference: Elliptic Equations

Elliptic equations in engineering are typically used to characterize steady-state, boundary-value problems. Before demonstrating how they can be solved, we will illustrate how a simple case—the Laplace equation—is derived from a physical problem context.

29.1 THE LAPLACE EQUATION

As mentioned in the introduction to this part of the book, the Laplace equation can be used to model a variety of problems involving the potential of an unknown variable. Because of its simplicity and general relevance to most areas of engineering, we will use a heated plate as our fundamental context for deriving and solving this elliptic PDE. Homework problems and engineering applications (Chap. 32) will be employed to illustrate the applicability of the model to other engineering problem contexts.

Figure 29.1 shows an element on the face of a thin rectangular plate of thickness Δz . The plate is insulated everywhere but at its edges, where the temperature can be set at a prescribed level. The insulation and the thinness of the plate mean that heat transfer is limited to the x and y dimensions. At steady state, the flow of heat into the element over a unit time period Δt must equal the flow out, as in

$$\begin{aligned} q(x) \Delta y \Delta z \Delta t + q(y) \Delta x \Delta z \Delta t &= q(x + \Delta x) \Delta y \Delta z \Delta t \\ &\quad + q(y + \Delta y) \Delta x \Delta z \Delta t \end{aligned} \tag{29.1}$$

where $q(x)$ and $q(y)$ = the heat fluxes at x and y , respectively [cal/(cm² · s)]. Dividing by Δz and Δt and collecting terms yields

$$[q(x) - q(x + \Delta x)]\Delta y + [q(y) - q(y + \Delta y)]\Delta x = 0$$

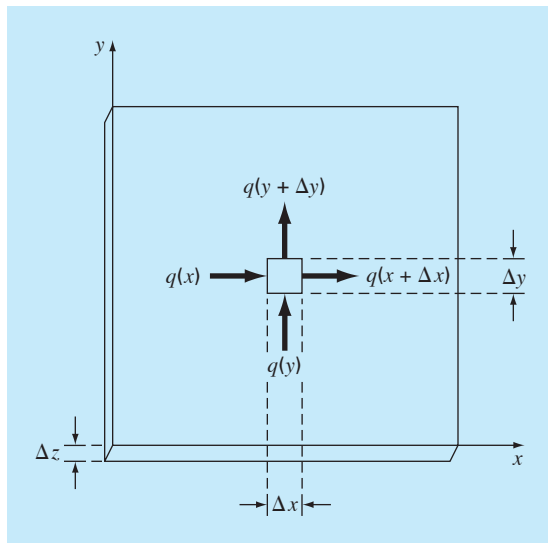
Multiplying the first term by $\Delta x / \Delta x$ and the second by $\Delta y / \Delta y$ gives

$$\frac{q(x) - q(x + \Delta x)}{\Delta x} \Delta x \Delta y + \frac{q(y) - q(y + \Delta y)}{\Delta y} \Delta y \Delta x = 0 \tag{29.2}$$

Dividing by $\Delta x \Delta y$ and taking the limit results in

$$-\frac{\partial q}{\partial x} - \frac{\partial q}{\partial y} = 0 \tag{29.3}$$

where the partial derivatives result from the definitions in Eqs. (PT7.1) and (PT7.2).

**FIGURE 29.1**

A thin plate of thickness Δz . An element is shown about which a heat balance is taken.

Equation (29.3) is a partial differential equation that is an expression of the conservation of energy for the plate. However, unless heat fluxes are specified at the plate's edges, it cannot be solved. Because temperature boundary conditions are given, Eq. (29.3) must be reformulated in terms of temperature. The link between flux and temperature is provided by *Fourier's law of heat conduction*, which can be represented as

$$q_i = -k\rho C \frac{\partial T}{\partial i} \quad (29.4)$$

where q_i = heat flux in the direction of the i dimension [cal/(cm² · s)], k = coefficient of thermal diffusivity (cm²/s), ρ = density of the material (g/cm³), C = heat capacity of the material [cal/(g · °C)], and T = temperature (°C), which is defined as

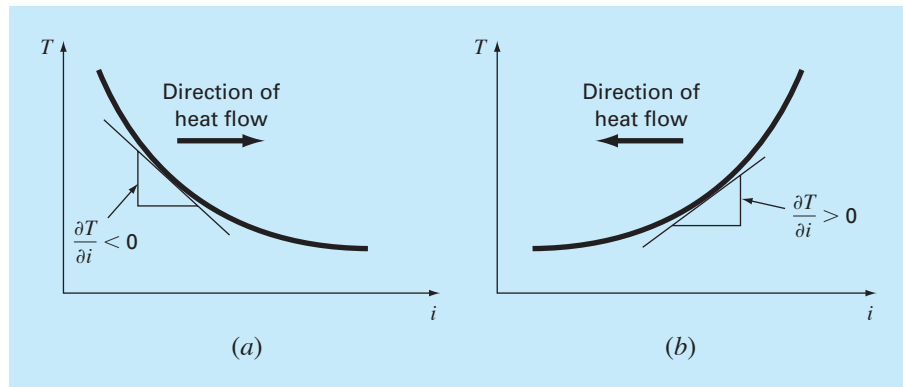
$$T = \frac{H}{\rho CV}$$

where H = heat (cal) and V = volume (cm³). Sometimes the term in front of the differential in Eq. (29.3) is treated as a single term,

$$k' = k\rho C \quad (29.5)$$

where k' is referred to as the *coefficient of thermal conductivity* [cal/(s · cm · °C)]. In either case, both k and k' are parameters that reflect how well the material conducts heat.

Fourier's law is sometimes referred to as a *constitutive equation*. It is given this label because it provides a mechanism that defines the system's internal interactions. Inspection

**FIGURE 29.2**

Graphical depiction of a temperature gradient. Because heat moves "downhill" from high to low temperature, the flow in (a) is from left to right in the positive i direction. However, due to the orientation of Cartesian coordinates, the slope is negative for this case. Thus, a negative gradient leads to a positive flow. This is the origin of the minus sign in Fourier's law of heat conduction. The reverse case is depicted in (b), where the positive gradient leads to a negative heat flow from right to left.

of Eq. (29.4) indicates that Fourier's law specifies that heat flux perpendicular to the i axis is proportional to the gradient or slope of temperature in the i direction. The negative sign ensures that a positive flux in the direction of i results from a negative slope from high to low temperature (Fig. 29.2). Substituting Eq. (29.4) into Eq. (29.3) results in

$$\frac{\partial^2 T}{\partial x^2} + \frac{\partial^2 T}{\partial y^2} = 0 \quad (29.6)$$

which is the *Laplace equation*. Note that for the case where there are sources or sinks of heat within the two-dimensional domain, the equation can be represented as

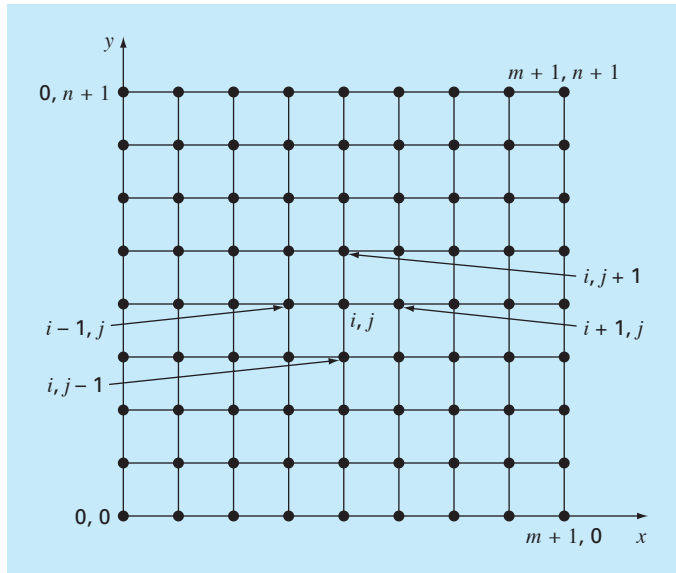
$$\frac{\partial^2 T}{\partial x^2} + \frac{\partial^2 T}{\partial y^2} = f(x, y) \quad (29.7)$$

where $f(x, y)$ is a function describing the sources or sinks of heat. Equation (29.7) is referred to as the *Poisson equation*.

29.2 SOLUTION TECHNIQUE

The numerical solution of elliptic PDEs such as the Laplace equation proceeds in the reverse manner of the derivation of Eq. (29.6) from the preceding section. Recall that the derivation of Eq. (29.6) employed a balance around a discrete element to yield an algebraic difference equation characterizing heat flux for a plate. Taking the limit turned this difference equation into a differential equation [Eq. (29.3)].

For the numerical solution, finite-difference representations based on treating the plate as a grid of discrete points (Fig. 29.3) are substituted for the partial derivatives in Eq. (29.6). As described next, the PDE is transformed into an algebraic difference equation.

**FIGURE 29.3**

A grid used for the finite-difference solution of elliptic PDEs in two independent variables such as the Laplace equation.

29.2.1 The Laplacian Difference Equation

Central differences based on the grid scheme from Fig. 29.3 are (recall Fig. 23.3)

$$\frac{\partial^2 T}{\partial x^2} = \frac{T_{i+1,j} - 2T_{i,j} + T_{i-1,j}}{\Delta x^2}$$

and

$$\frac{\partial^2 T}{\partial y^2} = \frac{T_{i,j+1} - 2T_{i,j} + T_{i,j-1}}{\Delta y^2}$$

which have errors of $O[\Delta(x)^2]$ and $O[\Delta(y)^2]$, respectively. Substituting these expressions into Eq. (29.6) gives

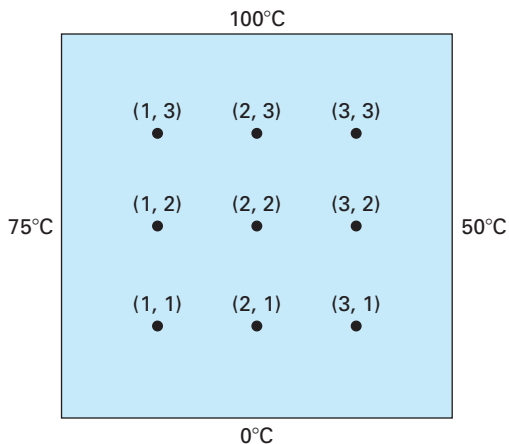
$$\frac{T_{i+1,j} - 2T_{i,j} + T_{i-1,j}}{\Delta x^2} + \frac{T_{i,j+1} - 2T_{i,j} + T_{i,j-1}}{\Delta y^2} = 0$$

For the square grid in Fig. 29.3, $\Delta x = \Delta y$, and by collection of terms, the equation becomes

$$T_{i+1,j} + T_{i-1,j} + T_{i,j+1} + T_{i,j-1} - 4T_{i,j} = 0 \quad (29.8)$$

This relationship, which holds for all interior points on the plate, is referred to as the *Laplacian difference equation*.

In addition, boundary conditions along the edges of the plate must be specified to obtain a unique solution. The simplest case is where the temperature at the boundary is set at a fixed value. This is called a *Dirichlet boundary condition*. Such is the case for Fig. 29.4,

**FIGURE 29.4**

A heated plate where boundary temperatures are held at constant levels. This case is called a Dirichlet boundary condition.

where the edges are held at constant temperatures. For the case illustrated in Fig. 29.4, a balance for node (1, 1) is, according to Eq. (29.8),

$$T_{21} + T_{01} + T_{12} + T_{10} - 4T_{11} = 0 \quad (29.9)$$

However, $T_{01} = 75$ and $T_{10} = 0$, and therefore, Eq. (29.9) can be expressed as

$$-4T_{11} + T_{12} + T_{21} = -75$$

Similar equations can be developed for the other interior points. The result is the following set of nine simultaneous equations with nine unknowns:

$$\begin{array}{ccccccccc}
 4T_{11} & -T_{21} & & -T_{12} & & & & & = 75 \\
 -T_{11} & +4T_{21} & -T_{31} & & -T_{22} & & & & = 0 \\
 & -T_{21} & +4T_{31} & & & -T_{32} & & & = 50 \\
 -T_{11} & & & +4T_{12} & -T_{22} & & -T_{13} & & = 75 \\
 & -T_{21} & & -T_{12} & +4T_{22} & -T_{32} & & -T_{23} & = 0 \\
 & & -T_{31} & & -T_{22} & +4T_{32} & & & -T_{33} = 50 \\
 & & & -T_{12} & & & +4T_{13} & -T_{23} & = 175 \\
 & & & -T_{22} & & -T_{13} & +4T_{23} & -T_{33} = 100 \\
 & & & -T_{32} & & -T_{23} & & +4T_{33} = 150
 \end{array} \quad (29.10)$$

29.2.2 The Liebmann Method

Most numerical solutions of the Laplace equation involve systems that are much larger than Eq. (29.10). For example, a 10-by-10 grid involves 100 linear algebraic equations. Solution techniques for these types of equations were discussed in Part Three.

Notice that there are a maximum of five unknown terms per line in Eq. (29.10). For larger-sized grids, this means that a significant number of the terms will be zero. When applied to such sparse systems, full-matrix elimination methods waste great amounts of computer memory storing these zeros. For this reason, approximate methods provide a viable approach for obtaining solutions for elliptical equations. The most commonly employed approach is *Gauss-Seidel*, which when applied to PDEs is also referred to as *Liebmann's method*. In this technique, Eq. (29.8) is expressed as

$$T_{i,j} = \frac{T_{i+1,j} + T_{i-1,j} + T_{i,j+1} + T_{i,j-1}}{4} \quad (29.11)$$

and solved iteratively for $j = 1$ to n and $i = 1$ to m . Because Eq. (29.8) is diagonally dominant, this procedure will eventually converge on a stable solution (recall Sec. 11.2.1). Overrelaxation is sometimes employed to accelerate the rate of convergence by applying the following formula after each iteration:

$$T_{i,j}^{\text{new}} = \lambda T_{i,j}^{\text{new}} + (1 - \lambda) T_{i,j}^{\text{old}} \quad (29.12)$$

where $T_{i,j}^{\text{new}}$ and $T_{i,j}^{\text{old}}$ are the values of $T_{i,j}$ from the present and the previous iteration, respectively, and λ is a weighting factor that is set between 1 and 2.

As with the conventional Gauss-Seidel method, the iterations are repeated until the absolute values of all the percent relative errors $(\varepsilon_a)_{i,j}$ fall below a prespecified stopping criterion ε_s . These percent relative errors are estimated by

$$|(\varepsilon_a)_{i,j}| = \left| \frac{T_{i,j}^{\text{new}} - T_{i,j}^{\text{old}}}{T_{i,j}^{\text{new}}} \right| 100\% \quad (29.13)$$

EXAMPLE 29.1

Temperature of a Heated Plate with Fixed Boundary Conditions

Problem Statement. Use Liebmann's method (Gauss-Seidel) to solve for the temperature of the heated plate in Fig. 29.4. Employ overrelaxation with a value of 1.5 for the weighting factor and iterate to $\varepsilon_s = 1\%$.

Solution. Equation (29.11) at $i = 1, j = 1$ is

$$T_{11} = \frac{0 + 75 + 0 + 0}{4} = 18.75$$

and applying overrelaxation yields

$$T_{11} = 1.5(18.75) + (1 - 1.5)0 = 28.125$$

For $i = 2, j = 1$,

$$T_{21} = \frac{0 + 28.125 + 0 + 0}{4} = 7.03125$$

$$T_{21} = 1.5(7.03125) + (1 - 1.5)0 = 10.54688$$

For $i = 3, j = 1$,

$$T_{31} = \frac{50 + 10.54688 + 0 + 0}{4} = 15.13672$$

$$T_{31} = 1.5(15.13672) + (1 - 1.5)0 = 22.70508$$

The computation is repeated for the other rows to give

$$\begin{array}{lll} T_{12} = 38.67188 & T_{22} = 18.45703 & T_{32} = 34.18579 \\ T_{13} = 80.12696 & T_{23} = 74.46900 & T_{33} = 96.99554 \end{array}$$

Because all the $T_{i,j}$'s are initially zero, all ε_a 's for the first iteration will be 100%.

For the second iteration the results are

$$\begin{array}{lll} T_{11} = 32.51953 & T_{21} = 22.35718 & T_{31} = 28.60108 \\ T_{12} = 57.95288 & T_{22} = 61.63333 & T_{32} = 71.86833 \\ T_{13} = 75.21973 & T_{23} = 87.95872 & T_{33} = 67.68736 \end{array}$$

The error for $T_{1,1}$ can be estimated as [Eq. (29.13)]

$$|(\varepsilon_a)_{1,1}| = \left| \frac{32.51953 - 28.12500}{32.51953} \right| 100\% = 13.5\%$$

Because this value is above the stopping criterion of 1%, the computation is continued. The ninth iteration gives the result

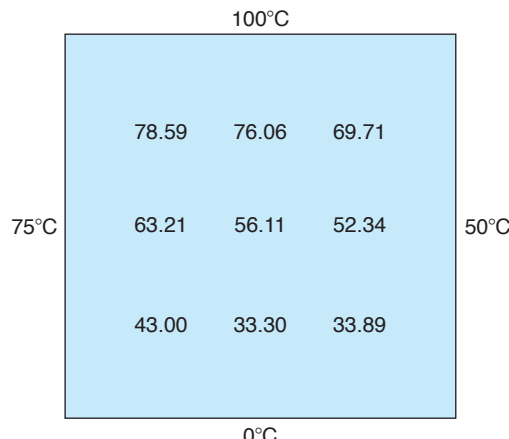
$$\begin{array}{lll} T_{11} = 43.00061 & T_{21} = 33.29755 & T_{31} = 33.88506 \\ T_{12} = 63.21152 & T_{22} = 56.11238 & T_{32} = 52.33999 \\ T_{13} = 78.58718 & T_{23} = 76.06402 & T_{33} = 69.71050 \end{array}$$

where the maximum error is 0.71%.

Figure 29.5 shows the results. As expected, a gradient is established as heat flows from high to low temperatures.

FIGURE 29.5

Temperature distribution for a heated plate subject to fixed boundary conditions.



29.2.3 Secondary Variables

Because its distribution is described by the Laplace equation, temperature is considered to be the primary variable in the heated-plate problem. For this case, as well as for other problems involving PDEs, secondary variables may also be of interest. As a matter of fact, in certain engineering contexts, the secondary variable may actually be more important.

For the heated plate, a secondary variable is the rate of heat flux across the plate's surface. This quantity can be computed from Fourier's law. Central finite-difference approximations for the first derivatives (recall Fig. 23.3) can be substituted into Eq. (29.4) to give the following values for heat flux in the x and y dimensions:

$$q_x = -k' \frac{T_{i+1,j} - T_{i-1,j}}{2 \Delta x} \quad (29.14)$$

and

$$q_y = -k' \frac{T_{i,j+1} - T_{i,j-1}}{2 \Delta y} \quad (29.15)$$

The resultant heat flux can be computed from these two quantities by

$$q_n = \sqrt{q_x^2 + q_y^2} \quad (29.16)$$

where the direction of q_n is given by

$$\theta = \tan^{-1} \left(\frac{q_y}{q_x} \right) \quad (29.17)$$

for $q_x > 0$ and

$$\theta = \tan^{-1} \left(\frac{q_y}{q_x} \right) + \pi \quad (29.18)$$

for $q_x < 0$. Recall that the angle can be expressed in degrees by multiplying it by $180^\circ/\pi$. If $q_x = 0$, θ is $\pi/2$ (90°) or $3\pi/2$ (270°), depending on whether q_y is positive or negative, respectively.

EXAMPLE 29.2

Flux Distribution for a Heated Plate

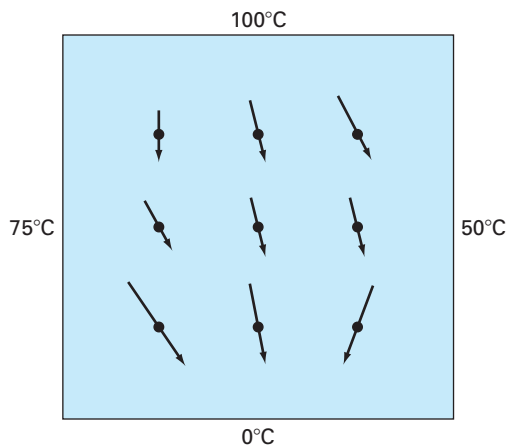
Problem Statement. Employ the results of Example 29.1 to determine the distribution of heat flux for the heated plate from Fig. 29.4. Assume that the plate is 40×40 cm and is made out of aluminum [$k' = 0.49 \text{ cal}/(\text{s} \cdot \text{cm} \cdot {}^\circ\text{C})$].

Solution. For $i = j = 1$, Eq. (29.14) can be used to compute

$$q_x = -0.49 \frac{\text{cal}}{\text{s} \cdot \text{cm} \cdot {}^\circ\text{C}} \frac{(33.29755 - 75)^\circ\text{C}}{2(10 \text{ cm})} = 1.022 \text{ cal}/(\text{cm}^2 \cdot \text{s})$$

and [Eq. (29.15)]

$$q_y = -0.49 \frac{\text{cal}}{\text{s} \cdot \text{cm} \cdot {}^\circ\text{C}} \frac{(63.21152 - 0)^\circ\text{C}}{2(10 \text{ cm})} = -1.549 \text{ cal}/(\text{cm}^2 \cdot \text{s})$$

**FIGURE 29.6**

Heat flux for a plate subject to fixed boundary temperatures. Note that the lengths of the arrows are proportional to the magnitude of the flux.

The resultant flux can be computed with Eq. (29.16):

$$q_n = \sqrt{(1.022)^2 + (-1.549)^2} = 1.856 \text{ cal}/(\text{cm}^2 \cdot \text{s})$$

and the angle of its trajectory by Eq. (29.17)

$$\theta = \tan^{-1} \left(\frac{-1.549}{1.022} \right) = -0.98758 \times \frac{180^\circ}{\pi} = -56.584^\circ$$

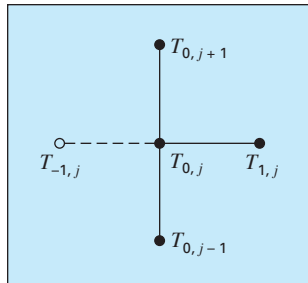
Thus, at this point, the heat flux is directed down and to the right. Values at the other grid points can be computed; the results are displayed in Fig. 29.6.

29.3 BOUNDARY CONDITIONS

Because it is free of complicating factors, the rectangular plate with fixed boundary conditions has been an ideal context for showing how elliptic PDEs can be solved numerically. We will now elaborate on other issues that will expand our capabilities to address more realistic problems. These involve boundaries at which the derivative is specified and boundaries that are irregularly shaped.

29.3.1 Derivative Boundary Conditions

The fixed or Dirichlet boundary condition discussed to this point is but one of several types that are used with partial differential equations. A common alternative is the case where the

**FIGURE 29.7**

A boundary node $(0, j)$ on the left edge of a heated plate. To approximate the derivative normal to the edge (that is, the x derivative), an imaginary point $(-1, j)$ is located a distance Δx beyond the edge.

derivative is given. This is commonly referred to as a *Neumann boundary condition*. For the heated-plate problem, this amounts to specifying the heat flux rather than the temperature at the boundary. One example is the situation where the edge is insulated. In this case, the derivative is zero. This conclusion is drawn directly from Eq. (29.4) because insulating a boundary means that the heat flux (and consequently the gradient) must be zero. Another example would be where heat is lost across the edge by predictable mechanisms such as radiation or convection.

Figure 29.7 depicts a node $(0, j)$ at the left edge of a heated plate. Applying Eq. (29.8) at the point gives

$$T_{1,j} + T_{-1,j} + T_{0,j+1} + T_{0,j-1} - 4T_{0,j} = 0 \quad (29.19)$$

Notice that an imaginary point $(-1, j)$ lying outside the plate is required for this equation. Although this exterior fictitious point might seem to represent a problem, it actually serves as the vehicle for incorporating the derivative boundary condition into the problem. This is done by representing the first derivative in the x dimension at $(0, j)$ by the finite divided difference

$$\frac{\partial T}{\partial x} \cong \frac{T_{1,j} - T_{-1,j}}{2 \Delta x}$$

which can be solved for

$$T_{-1,j} = T_{1,j} - 2 \Delta x \frac{\partial T}{\partial x}$$

Now we have a relationship for $T_{-1,j}$ that actually includes the derivative. It can be substituted into Eq. (29.19) to give

$$2T_{1,j} - 2 \Delta x \frac{\partial T}{\partial x} + T_{0,j+1} + T_{0,j-1} - 4T_{0,j} = 0 \quad (29.20)$$

Thus, we have incorporated the derivative into the balance.

Similar relationships can be developed for derivative boundary conditions at the other edges. The following example shows how this is done for the heated plate.

EXAMPLE 29.3

Heated Plate with an Insulated Edge

Problem Statement. Repeat the same problem as in Example 29.1, but with the lower edge insulated.

Solution. The general equation to characterize a derivative at the lower edge (that is, at $j = 0$) of a heated plate is

$$T_{i+1,0} + T_{i-1,0} + 2T_{i,1} - 2 \Delta y \frac{\partial T}{\partial y} - 4T_{i,0} = 0$$

For an insulated edge, the derivative is zero and the equation becomes

$$T_{i+1,0} + T_{i-1,0} + 2T_{i,1} - 4T_{i,0} = 0$$

The simultaneous equations for temperature distribution on the plate in Fig. 29.4 with an insulated lower edge can be written in matrix form as

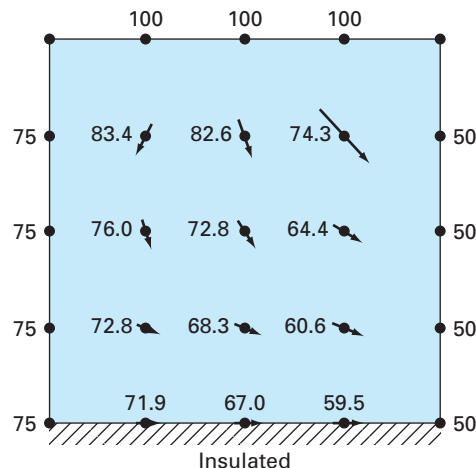
$$\left[\begin{array}{cccccc} 4 & -1 & -2 & & & \\ -1 & 4 & -1 & -2 & & \\ & -1 & 4 & & -2 & \\ -1 & & 4 & -1 & -1 & \\ -1 & & -1 & 4 & -1 & -1 \\ & -1 & & 4 & -1 & -1 \\ & & -1 & -1 & 4 & -1 \\ & & & -1 & -1 & 4 \\ & & & & -1 & -1 \\ & & & & & 4 & -1 \\ & & & & & -1 & -1 \\ & & & & & & -1 \end{array} \right] \begin{Bmatrix} T_{10} \\ T_{20} \\ T_{30} \\ T_{11} \\ T_{21} \\ T_{31} \\ T_{12} \\ T_{22} \\ T_{32} \\ T_{13} \\ T_{23} \\ T_{33} \end{Bmatrix} = \begin{Bmatrix} 75 \\ 0 \\ 50 \\ 75 \\ 0 \\ 50 \\ 75 \\ 0 \\ 50 \\ 175 \\ 100 \\ 150 \end{Bmatrix}$$

Note that because of the derivative boundary condition, the matrix is increased to 12×12 in contrast to the 9×9 system in Eq. (29.10) to account for the three unknown temperatures along the plate's lower edge. These equations can be solved for

$$\begin{aligned} T_{10} &= 71.91 & T_{20} &= 67.01 & T_{30} &= 59.54 \\ T_{11} &= 72.81 & T_{21} &= 68.31 & T_{31} &= 60.57 \\ T_{12} &= 76.01 & T_{22} &= 72.84 & T_{32} &= 64.42 \\ T_{13} &= 83.41 & T_{23} &= 82.63 & T_{33} &= 74.26 \end{aligned}$$

FIGURE 29.8

Temperature and flux distribution for a heated plate subject to fixed boundary conditions except for an insulated lower edge.



These results and computed fluxes (for the same parameters as in Example 29.2) are displayed in Fig. 29.8. Note that, because the lower edge is insulated, the plate's temperature is higher than for Fig. 29.5, where the bottom edge temperature is fixed at zero. In addition, the heat flow (in contrast to Fig. 29.6) is now deflected to the right and moves parallel to the insulated wall.

29.3.2 Irregular Boundaries

Although the rectangular plate from Fig. 29.4 has served well to illustrate the fundamental aspects of solving elliptic PDEs, many engineering problems do not exhibit such an idealized geometry. For example, a great many systems have irregular boundaries (Fig. 29.9).

Figure 29.9 is a system that can serve to illustrate how nonrectangular boundaries can be handled. As depicted, the plate's lower left boundary is circular. Notice that we have affixed parameters— $\alpha_1, \alpha_2, \beta_1, \beta_2$ —to each of the lengths surrounding the node. Of course, for the plate depicted in Fig. 29.9, $\alpha_2 = \beta_2 = 1$. However, we will retain these parameters throughout the following derivation so that the resulting equation is generally applicable to any irregular boundary—not just one on the lower left-hand corner of a heated plate. The first derivatives in the x dimension can be approximated as

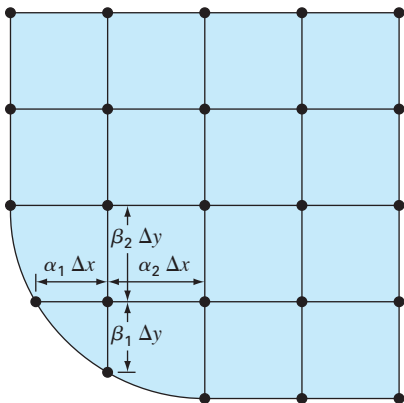
$$\left(\frac{\partial T}{\partial x} \right)_{i-1,i} \cong \frac{T_{i,j} - T_{i-1,j}}{\alpha_1 \Delta x} \quad (29.21)$$

and

$$\left(\frac{\partial T}{\partial x} \right)_{i,i+1} \cong \frac{T_{i+1,j} - T_{i,j}}{\alpha_2 \Delta x} \quad (29.22)$$

FIGURE 29.9

A grid for a heated plate with an irregularly shaped boundary. Note how weighting coefficients are used to account for the nonuniform spacing in the vicinity of the nonrectangular boundary.



The second derivatives can be developed from these first derivatives. For the x dimension, the second derivative is

$$\frac{\partial^2 T}{\partial x^2} = \frac{\partial}{\partial x} \left(\frac{\partial T}{\partial x} \right) = \frac{\left(\frac{\partial T}{\partial x} \right)_{i,i+1} - \left(\frac{\partial T}{\partial x} \right)_{i-1,i}}{\frac{\alpha_1 \Delta x + \alpha_2 \Delta x}{2}} \quad (29.23)$$

Substituting Eqs. (29.21) and (29.22) into (29.23) gives

$$\frac{\partial^2 T}{\partial x^2} = 2 \frac{\frac{T_{i-1,j} - T_{i,j}}{\alpha_1 \Delta x} - \frac{T_{i+1,j} - T_{i,j}}{\alpha_2 \Delta x}}{\alpha_1 \Delta x + \alpha_2 \Delta x}$$

Collecting terms yields

$$\frac{\partial^2 T}{\partial x^2} = \frac{2}{\Delta x^2} \left[\frac{T_{i-1,j} - T_{i,j}}{\alpha_1(\alpha_1 + \alpha_2)} + \frac{T_{i+1,j} - T_{i,j}}{\alpha_2(\alpha_1 + \alpha_2)} \right]$$

A similar equation can be developed in the y dimension:

$$\frac{\partial^2 T}{\partial y^2} = \frac{2}{\Delta y^2} \left[\frac{T_{i,j-1} - T_{i,j}}{\beta_1(\beta_1 + \beta_2)} + \frac{T_{i,j+1} - T_{i,j}}{\beta_2(\beta_1 + \beta_2)} \right]$$

Substituting these equations in Eq. (29.6) yields

$$\begin{aligned} & \frac{2}{\Delta x^2} \left[\frac{T_{i-1,j} - T_{i,j}}{\alpha_1(\alpha_1 + \alpha_2)} + \frac{T_{i+1,j} - T_{i,j}}{\alpha_2(\alpha_1 + \alpha_2)} \right] \\ & + \frac{2}{\Delta y^2} \left[\frac{T_{i,j-1} - T_{i,j}}{\beta_1(\beta_1 + \beta_2)} + \frac{T_{i,j+1} - T_{i,j}}{\beta_2(\beta_1 + \beta_2)} \right] = 0 \end{aligned} \quad (29.24)$$

As illustrated in the following example, Eq. (29.24) can be applied to any node that lies adjacent to an irregular, Dirichlet-type boundary.

EXAMPLE 29.4

Heated Plate with an Irregular Boundary

Problem Statement. Repeat the same problem as in Example 29.1, but with the lower edge as depicted in Fig. 29.9.

Solution. For the case in Fig. 29.9, $\Delta x = \Delta y$, $\alpha_1 = \beta_1 = 0.732$, and $\alpha_2 = \beta_2 = 1$. Substituting these values into Eq. (29.24) yields the following balance for node (1, 1):

$$\begin{aligned} & 0.788675(T_{01} - T_{11}) + 0.57735(T_{21} - T_{11}) \\ & + 0.788675(T_{10} - T_{11}) + 0.57735(T_{12} - T_{11}) = 0 \end{aligned}$$

Collecting terms, we can express this equation as

$$-4T_{11} + 0.8453T_{21} + 0.8453T_{12} = -1.1547T_{01} - 1.1547T_{10}$$

The simultaneous equations for temperature distribution on the plate in Fig. 29.9 with a lower-edge boundary temperature of 75 can be written in matrix form as

$$\left[\begin{array}{cccccc} 4 & -0.845 & & -0.845 & & \\ -1 & 4 & -1 & & -1 & \\ & -1 & 4 & & -1 & \\ -1 & & 4 & -1 & -1 & \\ & -1 & & 4 & -1 & -1 \\ & & -1 & & 4 & -1 \\ & & & -1 & & -1 \\ & & & & 4 & -1 \\ & & & & -1 & 4 \\ & & & & & -1 & -1 \\ & & & & & & -4 \end{array} \right] \begin{Bmatrix} T_{11} \\ T_{21} \\ T_{31} \\ T_{12} \\ T_{22} \\ T_{32} \\ T_{13} \\ T_{23} \\ T_{33} \end{Bmatrix} = \begin{Bmatrix} 173.2 \\ 75 \\ 125 \\ 75 \\ 0 \\ 50 \\ 175 \\ 100 \\ 150 \end{Bmatrix}$$

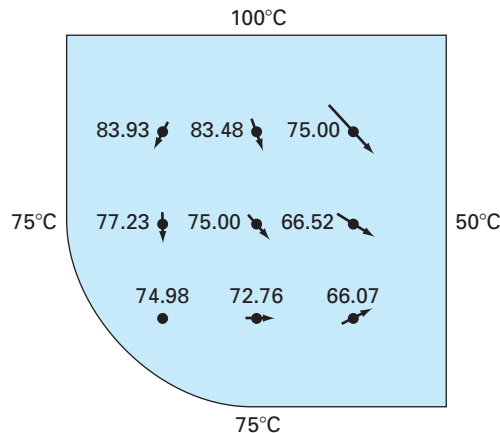
These equations can be solved for

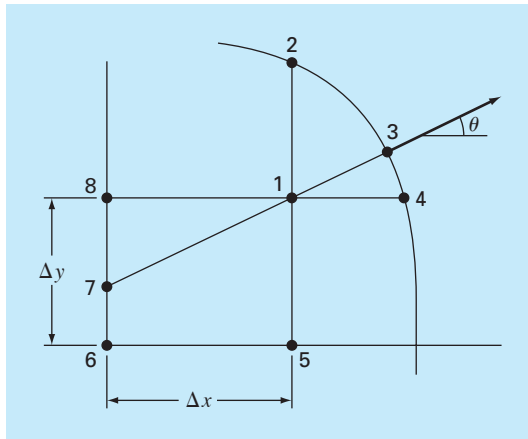
$$\begin{aligned} T_{11} &= 74.98 & T_{21} &= 72.76 & T_{31} &= 66.07 \\ T_{12} &= 77.23 & T_{22} &= 75.00 & T_{32} &= 66.52 \\ T_{13} &= 83.93 & T_{23} &= 83.48 & T_{33} &= 75.00 \end{aligned}$$

These results along with the computed fluxes are displayed in Fig. 29.10. Note that the fluxes are computed in the same fashion as in Sec. 29.2.3, with the exception that $(\alpha_1 + \alpha_2)$ and $(\beta_1 + \beta_2)$ are substituted for the 2's in the denominators of Eqs. (29.14) and (29.15), respectively. Section 32.3 illustrates how this is done.

FIGURE 29.10

Temperature and flux distribution for a heated plate with a circular boundary.



**FIGURE 29.11**

A curved boundary where the normal gradient is specified.

Derivative conditions for irregularly shaped boundaries are more difficult to formulate. Figure 29.11 shows a point near an irregular boundary where the normal derivative is specified.

The normal derivative at node 3 can be approximated by the gradient between nodes 1 and 7,

$$\left. \frac{\partial T}{\partial \eta} \right|_3 = \frac{T_1 - T_7}{L_{17}} \quad (29.25)$$

When θ is less than 45° as shown, the distance from node 7 to 8 is $\Delta x \tan \theta$, and linear interpolation can be used to estimate

$$T_7 = T_8 + (T_6 - T_8) \frac{\Delta x \tan \theta}{\Delta y}$$

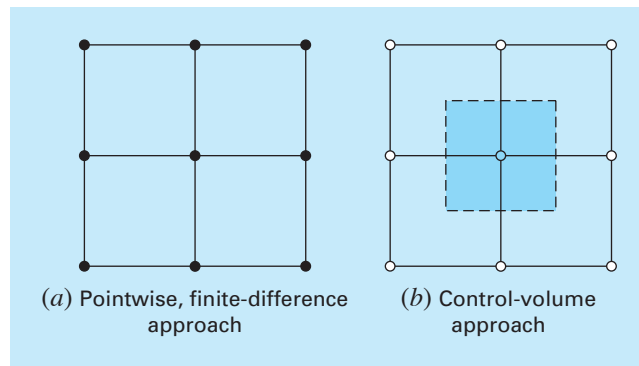
The length L_{17} is equal to $\Delta x / \cos \theta$. This length, along with the approximation for T_7 , can be substituted into Eq. (29.25) to give

$$T_1 = \left(\frac{\Delta x}{\cos \theta} \right) \left. \frac{\partial T}{\partial \eta} \right|_3 + T_6 \frac{\Delta x \tan \theta}{\Delta y} + T_8 \left(1 - \frac{\Delta x \tan \theta}{\Delta y} \right) \quad (29.26)$$

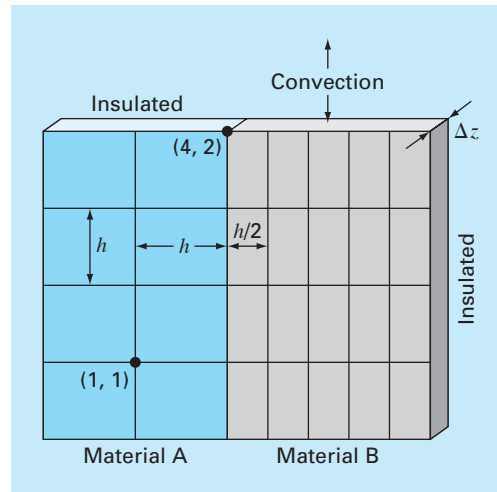
Such an equation provides a means for incorporating the normal gradient into the finite-difference approach. For cases where θ is greater than 45° , a different equation would be used. The determination of this formula will be left as a homework exercise.

29.4 THE CONTROL-VOLUME APPROACH

To summarize, the finite-difference or Taylor series approach divides the continuum into nodes (Fig. 29.12a). The underlying partial differential equation is written for each of these nodes. Finite-difference approximations are then substituted for the derivatives to convert the equations to an algebraic form.

**FIGURE 29.12**

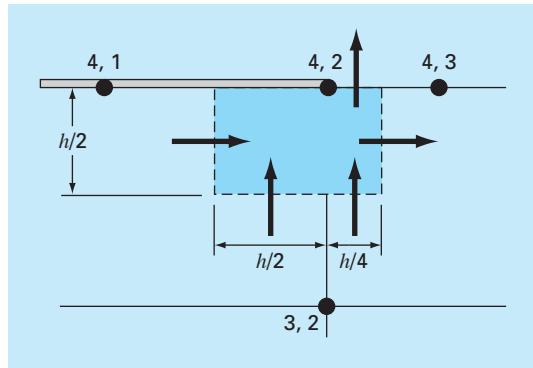
Two different perspectives for developing approximate solutions of PDEs: (a) finite-difference and (b) control volume.

**FIGURE 29.13**

A heated plate with unequal grid spacing, two materials, and mixed boundary conditions.

Such an approach is quite simple and straightforward for orthogonal (that is, rectangular) grids and constant coefficients. However, the approach becomes a more difficult endeavor for derivative conditions on irregularly shaped boundaries.

Figure 29.13 is an example of a system where additional difficulties arise. This plate is made of two different materials and has unequal grid spacing. In addition, half of its top edge is subject to convective heat transfer, whereas half is insulated. Developing equations for node (4, 2) would require some additional derivation beyond the approaches developed to this point.

**FIGURE 29.14**

A control volume for node (4, 2) with arrows indicating heat transfer through the boundaries.

The *control-volume approach* (also called the *volume-integral approach*) offers an alternative way to numerically approximate PDEs that is especially useful for cases such as Fig. 29.13. As in Fig. 29.12b, the approach resembles the point-wise approach in that points are determined across the domain. However, rather than approximating the PDE at a point, the approximation is applied to a volume surrounding the point. For an orthogonal grid, the volume is formed by the perpendicular lines through the midpoint of each line joining adjacent nodes. A heat balance can then be developed for each volume in a fashion similar to Eq. (29.1).

As an example, we will apply the control-volume approach to node (4, 2). First, the volume is defined by bisecting the lines joining the nodes. As in Fig. 29.14, the volume has conductive heat transfer through its left, right, and lower boundaries and convective heat transfer through half of its upper boundary. Notice that the transfer through the lower boundary involves both materials.

A steady-state heat balance for the volume can be written in qualitative terms as

$$0 = \left(\begin{array}{l} \text{left-side} \\ \text{conduction} \end{array} \right) - \left(\begin{array}{l} \text{right-side} \\ \text{conduction} \end{array} \right) + \left(\begin{array}{l} \text{lower conduction} \\ \text{material "a"} \end{array} \right) + \left(\begin{array}{l} \text{lower conduction} \\ \text{material "b"} \end{array} \right) - \left(\begin{array}{l} \text{upper} \\ \text{convection} \end{array} \right) \quad (29.27)$$

Now the conduction flux rate can be represented by the finite-difference version of Fourier's law. For example, for the left-side conduction gain, it would be

$$q = -k'_a \frac{T_{42} - T_{41}}{h}$$

where q has units of cal/cm²/s. This flux rate must be then multiplied by the area across which it enters ($\Delta z \times h/2$) to give the rate of heat entering the volume per unit time,

$$Q = -k'_a \frac{T_{42} - T_{41}}{h} \frac{h}{2} \Delta z$$

where Q has units of cal/s.

The heat flux due to convection can be formulated as

$$q = h_c(T_a - T_{42})$$

where h_c = a heat convection coefficient [cal/(s · cm² · °C)] and T_a = the air temperature (°C). Again, multiplication by the proper area yields the rate of heat flow per time,

$$Q = h_c(T_a - T_{42}) \frac{h}{4} \Delta z$$

The other transfers can be developed in a similar fashion and substituted into Eq. (29.27) to yield

$$0 = -k'_a \frac{T_{42} - T_{41}}{h} \frac{h}{2} \Delta z + k'_b \frac{T_{43} - T_{42}}{h/2} \frac{h}{2} \Delta z$$

(left-side conduction) (right-side conduction)

$$-k'_a \frac{T_{42} - T_{32}}{h} \frac{h}{2} \Delta z - k'_b \frac{T_{42} - T_{32}}{h} \frac{h}{4} \Delta z + h_c(T_a - T_{42}) \frac{h}{4} \Delta z$$

$\begin{pmatrix} \text{lower conduction} \\ \text{material "a"} \end{pmatrix} \begin{pmatrix} \text{lower conduction} \\ \text{material "b"} \end{pmatrix}$ (upper convection)

Parameter values can then be substituted to yield the final heat balance equation. For example, if $\Delta z = 0.5$ cm, $h = 10$ cm, $k'_a = 0.3$ cal/(s · cm · °C), $k'_b = 0.5$ cal/(s · cm · °C), and $h_c = 0.1$ cal/(s · cm² · °C), the equation becomes

$$0.5875T_{42} - 0.075T_{41} - 0.25T_{43} - 0.1375T_{32} = 2.5$$

To make the equation comparable to the standard Laplacian, this equation can be multiplied by 4/0.5875 so that the coefficient of the base node has a coefficient of 4,

$$4T_{42} - 0.510638T_{41} - 1.702128T_{43} - 0.93617T_{32} = 17.02128$$

For the standard cases covered to this point, the control-volume and pointwise finite-difference approaches yield identical results. For example, for node (1, 1) in Fig. 29.13, the balance would be

$$0 = -k'_a \frac{T_{11} - T_{01}}{h} h \Delta z + k'_a \frac{T_{21} - T_{11}}{h} h \Delta z - k'_a \frac{T_{11} - T_{10}}{h} h \Delta z + k'_a \frac{T_{12} - T_{11}}{h} h \Delta z$$

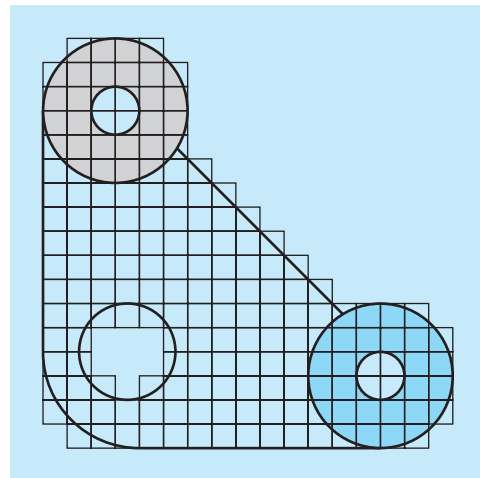
which simplifies to the standard Laplacian,

$$0 = 4T_{11} - T_{01} - T_{21} - T_{12} - T_{10}$$

We will look at other standard cases (for example, the derivative boundary condition) and explore the control-volume approach in additional detail in the problems at the end of this chapter.

29.5 SOFTWARE TO SOLVE ELLIPTIC EQUATIONS

Modifying a computer program to include derivative boundary conditions for rectangular systems is a relatively straightforward task. It merely involves ensuring that additional equations are generated to characterize the boundary nodes at which the derivatives are specified. In addition, the code must be modified so that these equations incorporate the derivative as seen in Eq. (29.20).

**FIGURE 29.15**

A finite-difference grid superimposed on an irregularly shaped gasket.

Developing general software to characterize systems with irregular boundaries is a much more difficult proposition. For example, a fairly involved algorithm would be required to model the simple gasket depicted in Fig. 29.15. This would involve two major modifications. First, a scheme would have to be developed to conveniently input the configuration of the nodes and to identify which were at the boundary. Second, an algorithm would be required to generate the proper simultaneous equations on the basis of the input information. The net result is that general software for solving elliptic (and for that matter, all) PDEs is relatively complicated.

One method used to simplify such efforts is to require a very fine grid. For such cases, it is often assumed that the closest node serves as the boundary point. In this way, the analysis does not have to consider the weighting parameters from Sec. 29.3.2. Although this introduces some error, the use of a sufficiently fine mesh can make the resulting discrepancy negligible. However, this involves a trade-off due to the computational burden introduced by the increased number of simultaneous equations.

As a consequence of these considerations, numerical analysts have developed alternative approaches that differ radically from finite-difference methods. Although these finite-element methods are more conceptually difficult, they can much more easily accommodate irregular boundaries. We will turn to these methods in Chap. 31. Before doing this, however, we will first describe finite-difference approaches for another category of PDEs—parabolic equations.

PROBLEMS

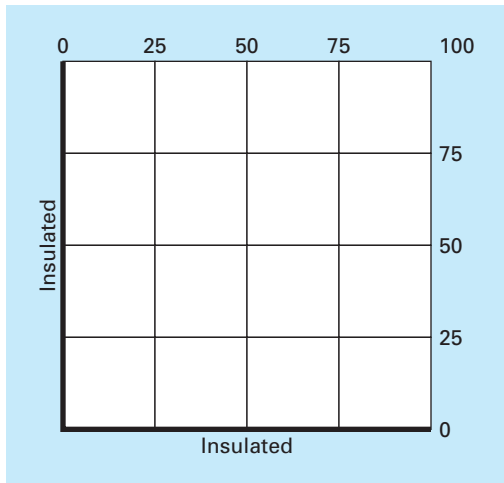
29.1 Use Liebmann's method to solve for the temperature of the square heated plate in Fig. 29.4, but with the upper boundary condition increased to 150°C and the left boundary insulated. Use a relaxation factor of 1.2 and iterate to $\varepsilon_s = 1\%$.

29.2 Use Liebmann's method to solve for the temperature of the square heated plate in Fig. 29.4, but with the upper boundary con-

dition increased to 120°C and the left boundary decreased to 60°C . Use a relaxation factor of 1.2 and iterate to $\varepsilon_s = 1\%$.

29.3 Compute the fluxes for Prob. 29.2 using the parameters from Example 29.3.

29.4 Repeat Example 29.1, but use 49 interior nodes (that is, $\Delta x = \Delta y = 5 \text{ cm}$).

**Figure P29.8**

29.5 Repeat Prob. 29.4, but for the case where the lower edge is insulated.

29.6 Repeat Examples 29.1 and 29.3, but for the case where the flux at the lower edge is directed downward with a value of $2 \text{ cal/cm}^2 \cdot \text{s}$.

29.7 Repeat Example 29.4 for the case where both the lower left and the upper right corners are rounded in the same fashion as the lower left corner of Fig. 29.9. Note that all boundary temperatures on the upper and right sides are fixed at 100°C and all on the lower and left sides are fixed at 50°C .

29.8 With the exception of the boundary conditions, the plate in Fig. P29.8 has the exact same characteristics as the plate used in Examples 23.1 through 23.4. Simulate both the temperatures and fluxes for the plate.

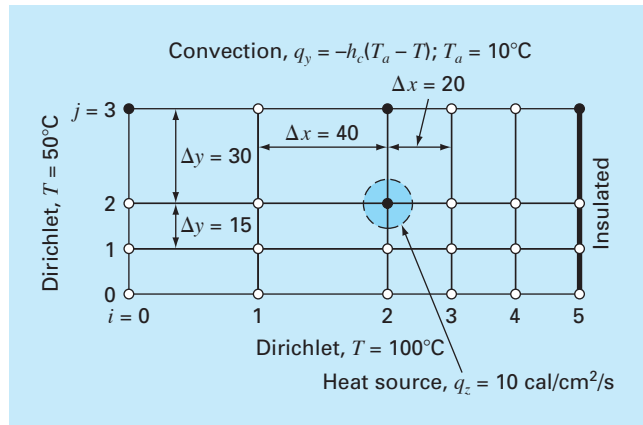
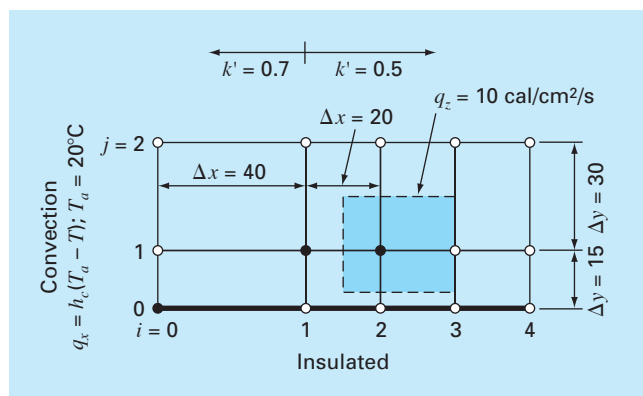
29.9 Write equations for the darkened nodes in the grid in Fig. P29.9. Note that all units are cgs. The coefficient of thermal conductivity for the plate is $0.75 \text{ cal/(s \cdot cm \cdot }^\circ\text{C)}$, the convection coefficient is $h_c = 0.015 \text{ cal/(cm}^2 \cdot \text{C} \cdot \text{s)}$, and the thickness of the plate is 0.5 cm.

29.10 Write equations for the darkened nodes in the grid in Fig. P29.10. Note that all units are cgs. The convection coefficient is $h_c = 0.01 \text{ cal/(cm}^2 \cdot \text{C} \cdot \text{s)}$ and the thickness of the plate is 2 cm.

29.11 Apply the control volume approach to develop the equation for node $(0, j)$ in Fig. 29.7.

29.12 Derive an equation like Eq. (29.26) for the case where θ is greater than 45° for Fig. 29.11.

29.13 Develop a user-friendly computer program to implement Liebmann's method for a rectangular plate with Dirichlet boundary conditions. Design the program so that it can compute both

**Figure P29.9****Figure P29.10**

temperature and flux. Test the program by duplicating the results of Examples 29.1 and 29.2.

29.14 Employ the program from Prob. 29.13 to solve Probs. 29.2 and 29.3.

29.15 Employ the program from Prob 29.13 to solve Prob. 29.4.

29.16 Use the control-volume approach and derive the node equation for node $(2, 2)$ in Fig. 29.13 and include a heat source at this point. Use the following values for the constants: $\Delta z = 0.25 \text{ cm}$, $h = 10 \text{ cm}$, $k_A = 0.25 \text{ W/cm} \cdot \text{C}$, and $k_B = 0.45 \text{ W/cm} \cdot \text{C}$. The heat source comes only from material A at the rate of $= 6 \text{ W/cm}^3$.

29.17 Calculate heat flux (W/cm^2) for node $(2, 2)$ in Fig. 29.13 using finite-difference approximations for the temperature gradients

at this node. Calculate the flux in the horizontal direction in materials A and B, and determine if these two fluxes should be equal. Also, calculate the vertical flux in materials A and B. Should these two fluxes be equal? Use the following values for the constants: $\Delta z = 0.5 \text{ cm}$, $h = 10 \text{ cm}$, $k_A = 0.25 \text{ W/cm} \cdot \text{C}$, $k_B = 0.45 \text{ W/cm} \cdot \text{C}$, and nodal temperatures: $T_{22} = 51.6^\circ\text{C}$, $T_{21} = 74.2^\circ\text{C}$, $T_{23} = 45.3^\circ\text{C}$, $T_{32} = 38.6^\circ\text{C}$, and $T_{12} = 87.4^\circ\text{C}$.

29.18 Compute the temperature distribution for the L-shaped plate in Fig. P29.18.

29.19 The Poisson equation can be written in three dimensions as

$$\frac{\partial^2 T}{\partial x^2} + \frac{\partial^2 T}{\partial y^2} + \frac{\partial^2 T}{\partial z^2} = f(x, y, z)$$

Solve for the distribution of temperature within a unit (1×1) cube with zero boundary conditions and $f = -10$. Employ $\Delta x = \Delta y = \Delta z = 1/6$.

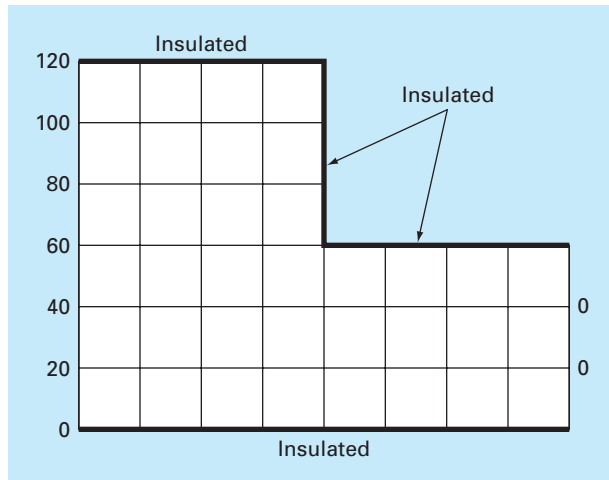


Figure P29.18

Finite Difference: Parabolic Equations

Chapter 29 dealt with steady-state PDEs. We now turn to the parabolic equations that are employed to characterize time-variable problems. In the latter part of this chapter, we will illustrate how this is done in two spatial dimensions for the heated plate. Before doing this, we will first show how the simpler one-dimensional case is approached.

30.1 THE HEAT-CONDUCTION EQUATION

In a fashion similar to the derivation of the Laplace equation [Eq. (29.6)], conservation of heat can be used to develop a heat balance for the differential element in the long, thin insulated rod shown in Fig. 30.1. However, rather than examine the steady-state case, the present balance also considers the amount of heat stored in the element over a unit time period Δt . Thus, the balance is in the form, inputs – outputs = storage, or

$$q(x) \Delta y \Delta z \Delta t - q(x + \Delta x) \Delta y \Delta z \Delta t = \Delta x \Delta y \Delta z \rho C \Delta T$$

Dividing by the volume of the element ($= \Delta x \Delta y \Delta z$) and Δt gives

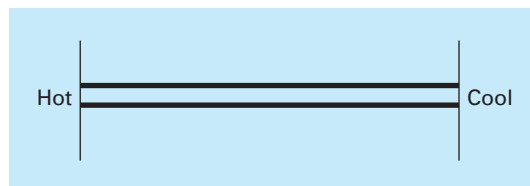
$$\frac{q(x) - q(x + \Delta x)}{\Delta x} = \rho C \frac{\Delta T}{\Delta t}$$

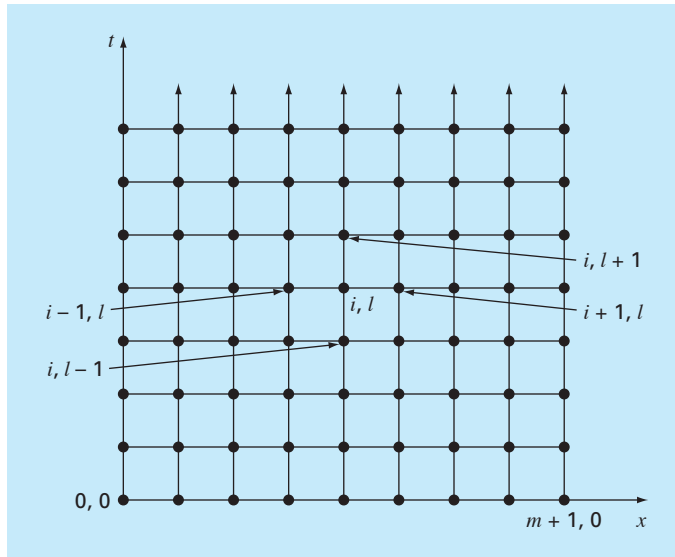
Taking the limit yields

$$-\frac{\partial q}{\partial x} = \rho C \frac{\partial T}{\partial t}$$

FIGURE 30.1

A thin rod, insulated at all points except at its ends.



**FIGURE 30.2**

A grid used for the finite-difference solution of parabolic PDEs in two independent variables such as the heat-conduction equation. Note how, in contrast to Fig. 29.3, this grid is open-ended in the temporal dimension.

Substituting Fourier's law of heat conduction [Eq. (29.4)] results in

$$k \frac{\partial^2 T}{\partial x^2} = \frac{\partial T}{\partial t} \quad (30.1)$$

which is the *heat-conduction equation*.

Just as with elliptic PDEs, parabolic equations can be solved by substituting finite divided differences for the partial derivatives. However, in contrast to elliptic PDEs, we must now consider changes in time as well as in space. Whereas elliptic equations were bounded in all relevant dimensions, parabolic PDEs are temporally open-ended (Fig. 30.2). Because of their time-variable nature, solutions to these equations involve a number of new issues, notably stability. This, as well as other aspects of parabolic PDEs, will be examined in the following sections as we present two fundamental solution approaches—explicit and implicit schemes.

30.2 EXPLICIT METHODS

The heat-conduction equation requires approximations for the second derivative in space and the first derivative in time. The former is represented in the same fashion as for the Laplace equation by a centered finite-divided difference:

$$\frac{\partial^2 T}{\partial x^2} = \frac{T_{i+1}^l - 2T_i^l + T_{i-1}^l}{\Delta x^2} \quad (30.2)$$

which has an error (recall Fig. 23.3) of $O[(\Delta x)^2]$. Notice the slight change in notation of the superscripts is used to denote time. This is done so that a second subscript can be used to designate a second spatial dimension when the approach is expanded to two spatial dimensions.

A forward finite-divided difference is used to approximate the time derivative

$$\frac{\partial T}{\partial t} = \frac{T_i^{l+1} - T_i^l}{\Delta t} \quad (30.3)$$

which has an error (recall Fig. 23.1) of $O(\Delta t)$.

Substituting Eqs. (30.2) and (30.3) into Eq. (30.1) yields

$$k \frac{T_{i+1}^l - 2T_i^l + T_{i-1}^l}{(\Delta x)^2} = \frac{T_i^{l+1} - T_i^l}{\Delta t} \quad (30.4)$$

which can be solved for

$$T_i^{l+1} = T_i^l + \lambda(T_{i+1}^l - 2T_i^l + T_{i-1}^l) \quad (30.5)$$

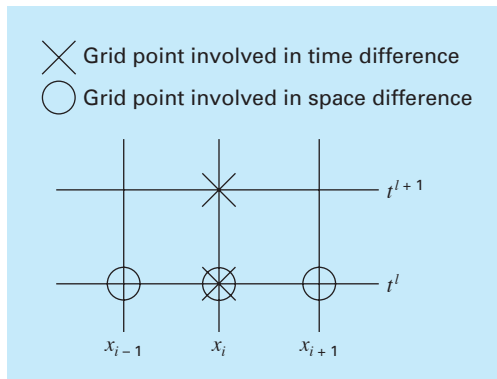
where $\lambda = k \Delta t / (\Delta x)^2$.

This equation can be written for all the interior nodes on the rod. It then provides an explicit means to compute values at each node for a future time based on the present values at the node and its neighbors. Notice that this approach is actually a manifestation of Euler's method for solving systems of ODEs. That is, if we know the temperature distribution as a function of position at an initial time, we can compute the distribution at a future time based on Eq. (30.5).

A computational molecule for the explicit method is depicted in Fig. 30.3, showing the nodes that constitute the spatial and temporal approximations. This molecule can be contrasted with others in this chapter to illustrate the differences between approaches.

FIGURE 30.3

A computational molecule for the explicit form.



EXAMPLE 30.1

Explicit Solution of the One-Dimensional Heat-Conduction Equation

Problem Statement. Use the explicit method to solve for the temperature distribution of a long, thin rod with a length of 10 cm and the following values: $k' = 0.49 \text{ cal/(s} \cdot \text{cm} \cdot ^\circ\text{C)}$, $\Delta x = 2 \text{ cm}$, and $\Delta t = 0.1 \text{ s}$. At $t = 0$, the temperature of the rod is zero and the boundary conditions are fixed for all times at $T(0) = 100^\circ\text{C}$ and $T(10) = 50^\circ\text{C}$. Note that the rod is aluminum with $C = 0.2174 \text{ cal/(g} \cdot ^\circ\text{C)}$ and $\rho = 2.7 \text{ g/cm}^3$. Therefore, $k = 0.49/(2.7 \cdot 0.2174) = 0.835 \text{ cm}^2/\text{s}$ and $\lambda = 0.835(0.1)/(2)^2 = 0.020875$.

Solution. Applying Eq. (30.5) gives the following value at $t = 0.1 \text{ s}$ for the node at $x = 2 \text{ cm}$:

$$T_1^1 = 0 + 0.020875[0 - 2(0) + 100] = 2.0875$$

At the other interior points, $x = 4, 6$, and 8 cm , the results are

$$T_2^1 = 0 + 0.020875[0 - 2(0) + 0] = 0$$

$$T_3^1 = 0 + 0.020875[0 - 2(0) + 0] = 0$$

$$T_4^1 = 0 + 0.020875[50 - 2(0) + 0] = 1.0438$$

At $t = 0.2 \text{ s}$, the values at the four interior nodes are computed as

$$T_1^2 = 2.0875 + 0.020875[0 - 2(2.0875) + 100] = 4.0878$$

$$T_2^2 = 0 + 0.020875[0 - 2(0) + 2.0875] = 0.043577$$

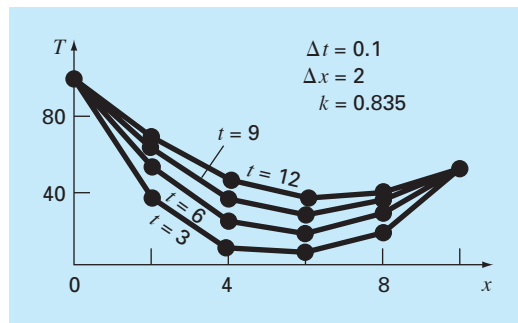
$$T_3^2 = 0 + 0.020875[1.0438 - 2(0) + 0] = 0.021788$$

$$T_4^2 = 1.0438 + 0.020875[50 - 2(1.0438) + 0] = 2.0439$$

The computation is continued, and the results at 3-s intervals are depicted in Fig. 30.4. The general rise in temperature with time indicates that the computation captures the diffusion of heat from the boundaries into the bar.

FIGURE 30.4

Temperature distribution in a long, thin rod as computed with the explicit method described in Sec. 30.2.



30.2.1 Convergence and Stability

Convergence means that as Δx and Δt approach zero, the results of the finite-difference technique approach the true solution. *Stability* means that errors at any stage of the computation are not amplified but are attenuated as the computation progresses. It can be shown (Carnahan et al., 1969) that the explicit method is both convergent and stable if $\lambda \leq 1/2$, or

$$\Delta t \leq \frac{1}{2} \frac{\Delta x^2}{k} \quad (30.6)$$

In addition, it should be noted that setting $\lambda \leq 1/2$ could result in a solution in which errors do not grow, but oscillate. Setting $\lambda \leq 1/4$ ensures that the solution will not oscillate. It is also known that setting $\lambda = 1/6$ tends to minimize truncation error (Carnahan et al., 1969).

Figure 30.5 is an example of instability caused by violating Eq. (30.6). This plot is for the same case as in Example 30.1 but with $\lambda = 0.735$, which is considerably greater than 0.5. As in Fig. 30.5, the solution undergoes progressively increasing oscillations. This situation will continue to deteriorate as the computation continues.

Although satisfaction of Eq. (30.6) will alleviate the instabilities of the sort manifested in Fig. 30.5, it also places a strong limitation on the explicit method. For example, suppose that Δx is halved to improve the approximation of the spatial second derivative. According to Eq. (30.6), the time step must be quartered to maintain convergence and stability. Thus, to perform comparable computations, the time steps must be increased by a factor of 4. Furthermore, the computation for each of these time steps will take twice as long because halving Δx doubles the total number of nodes for which equations must be written. Consequently, for the one-dimensional case, halving Δx results in an eightfold increase in the number of calculations. Thus, the computational burden may be large to attain acceptable accuracy. As will be described shortly, other techniques are available that do not suffer from such severe limitations.

30.2.2 Derivative Boundary Conditions

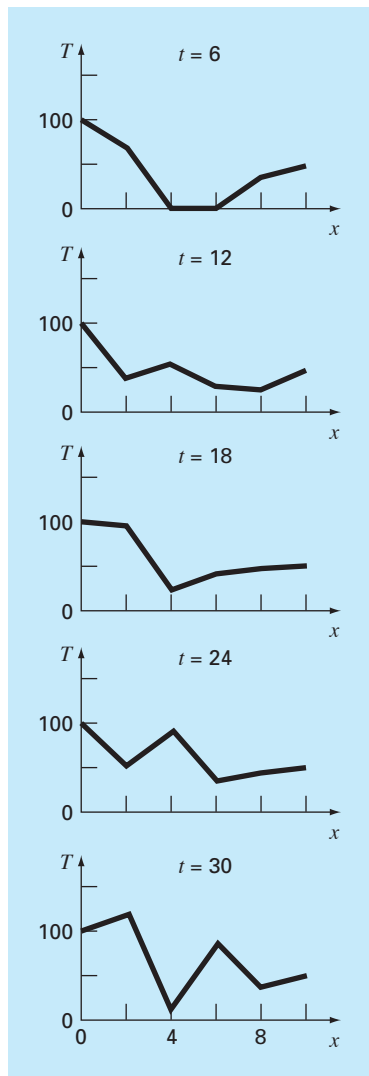
As was the case for elliptic PDEs (recall Sec. 29.3.1), derivative boundary conditions can be readily incorporated into parabolic equations. For a one-dimensional rod, this necessitates adding two equations to characterize the heat balance at the end nodes. For example, the node at the left end ($i = 0$) would be represented by

$$T_0^{l+1} = T_0^l + \lambda(T_1^l - 2T_0^l + T_{-1}^l)$$

Thus, an imaginary point is introduced at $i = -1$ (recall Fig. 29.7). However, as with the elliptic case, this point provides a vehicle for incorporating the derivative boundary condition into the analysis. Problem 30.2 at the end of the chapter deals with this exercise.

30.2.3 Higher-Order Temporal Approximations

The general idea of reexpressing the PDE as a system of ODEs is sometimes called the *method of lines*. Obviously, one way to improve on the Euler approach used above would be to employ a more accurate integration scheme for solving the ODEs. For example, the Heun method can be employed to obtain second-order temporal accuracy. An example of

**FIGURE 30.5**

An illustration of instability. Solution of Example 30.1 but with $\lambda = 0.735$.

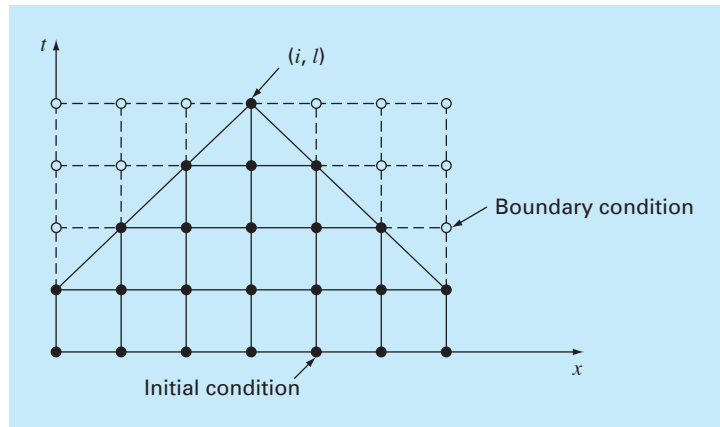
this approach is called *MacCormack's method*. This and other improved explicit methods are discussed elsewhere (for example, Hoffman, 1992).

30.3 A SIMPLE IMPLICIT METHOD

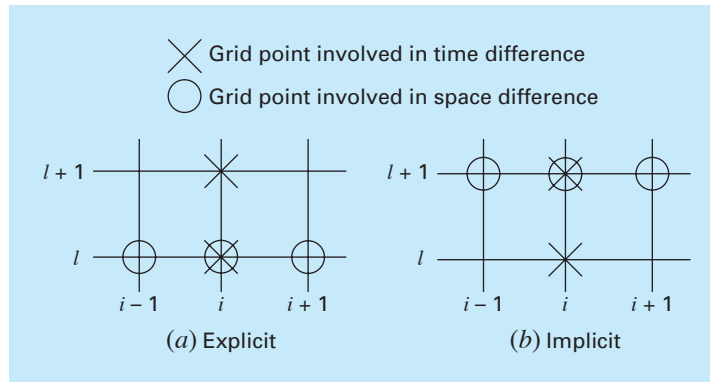
As noted previously, explicit finite-difference formulations have problems related to stability. In addition, as depicted in Fig. 30.6, they exclude information that has a bearing on the solution. Implicit methods overcome both these difficulties at the expense of somewhat more complicated algorithms.

FIGURE 30.6

Representation of the effect of other nodes on the finite-difference approximation at node (i, l) using an explicit finite-difference scheme. The shaded nodes have an influence on (i, l) , whereas the unshaded nodes, which in reality affect (i, l) , are excluded.

**FIGURE 30.7**

Computational molecules demonstrating the fundamental differences between (a) explicit and (b) implicit methods.



The fundamental difference between explicit and implicit approximations is depicted in Fig. 30.7. For the explicit form, we approximate the spatial derivative at time level l (Fig. 30.7a). Recall that when we substituted this approximation into the partial differential equation, we obtained a difference equation (30.4) with a single unknown T_i^{l+1} . Thus, we can solve “explicitly” for this unknown as in Eq. (30.5).

In implicit methods, the spatial derivative is approximated at an advanced time level $l + 1$. For example, the second derivative would be approximated by (Fig. 30.7b)

$$\frac{\partial^2 T}{\partial x^2} \cong \frac{T_{i+1}^{l+1} - 2T_i^{l+1} + T_{i-1}^{l+1}}{(\Delta x)^2} \quad (30.7)$$

which is second-order accurate. When this relationship is substituted into the original PDE, the resulting difference equation contains several unknowns. Thus, it cannot be solved

explicitly by simple algebraic rearrangement as was done in going from Eq. (30.4) to (30.5). Instead, the entire system of equations must be solved simultaneously. This is possible because, along with the boundary conditions, the implicit formulations result in a set of linear algebraic equations with the same number of unknowns. Thus, the method reduces to the solution of a set of simultaneous equations at each point in time.

To illustrate how this is done, substitute Eqs. (30.3) and (30.7) into Eq. (30.1) to give

$$k \frac{T_{i+1}^{l+1} - 2T_i^{l+1} + T_{i-1}^{l+1}}{(\Delta x)^2} = \frac{T_i^{l+1} - T_i^l}{\Delta t}$$

which can be expressed as

$$-\lambda T_{i-1}^{l+1} + (1 + 2\lambda) T_i^{l+1} - \lambda T_{i+1}^{l+1} = T_i^l \quad (30.8)$$

where $\lambda = k \Delta t / (\Delta x)^2$. This equation applies to all but the first and the last interior nodes, which must be modified to reflect the boundary conditions. For the case where the temperature levels at the ends of the rod are given, the boundary condition at the left end of the rod ($i = 0$) can be expressed as

$$T_0^{l+1} = f_0(t^{l+1}) \quad (30.9)$$

where $f_0(t^{l+1})$ = a function describing how the boundary temperature changes with time. Substituting Eq. (30.9) into Eq. (30.8) gives the difference equation for the first interior node ($i = 1$):

$$(1 + 2\lambda) T_1^{l+1} - \lambda T_2^{l+1} = T_1^l + \lambda f_0(t^{l+1}) \quad (30.10)$$

Similarly, for the last interior node ($i = m$),

$$-\lambda T_{m-1}^{l+1} + (1 + 2\lambda) T_m^{l+1} = T_m^l + \lambda f_{m+1}(t^{l+1}) \quad (30.11)$$

where $f_{m+1}(t^{l+1})$ describes the specified temperature changes at the right end of the rod ($i = m + 1$).

When Eqs. (30.8), (30.10), and (30.11) are written for all the interior nodes, the resulting set of m linear algebraic equations has m unknowns. In addition, the method has the added bonus that the system is tridiagonal. Thus, we can utilize the extremely efficient solution algorithms (recall Sec. 11.1.1) that are available for tridiagonal systems.

EXAMPLE 30.2

Simple Implicit Solution of the Heat-Conduction Equation

Problem Statement. Use the simple implicit finite-difference approximation to solve the same problem as in Example 30.1.

Solution. For the rod from Example 30.1, $\lambda = 0.020875$. Therefore, at $t = 0$, Eq. (30.10) can be written for the first interior node as

$$1.04175T_1^1 - 0.020875T_2^1 = 0 + 0.020875(100)$$

or

$$1.04175T_1^1 - 0.020875T_2^1 = 2.0875$$

In a similar fashion, Eqs. (30.8) and (30.11) can be applied to the other interior nodes. This leads to the following set of simultaneous equations:

$$\begin{bmatrix} 1.04175 & -0.020875 & & \\ -0.020875 & 1.04175 & -0.020875 & \\ & -0.020875 & 1.04175 & -0.020875 \\ & & -0.020875 & 1.04175 \end{bmatrix} \begin{Bmatrix} T_1^1 \\ T_2^1 \\ T_3^1 \\ T_4^1 \end{Bmatrix} = \begin{Bmatrix} 2.0875 \\ 0 \\ 0 \\ 1.04375 \end{Bmatrix}$$

which can be solved for the temperature at $t = 0.1$ s:

$$T_1^1 = 2.0047$$

$$T_2^1 = 0.0406$$

$$T_3^1 = 0.0209$$

$$T_4^1 = 1.0023$$

Notice how in contrast to Example 30.1, all the points have changed from the initial condition during the first time step.

To solve for the temperatures at $t = 0.2$, the right-hand-side vector must be modified to account for the results of the first step, as in

$$\begin{Bmatrix} 4.09215 \\ 0.04059 \\ 0.02090 \\ 2.04069 \end{Bmatrix}$$

The simultaneous equations can then be solved for the temperatures at $t = 0.2$ s:

$$T_1^2 = 3.9305$$

$$T_2^2 = 0.1190$$

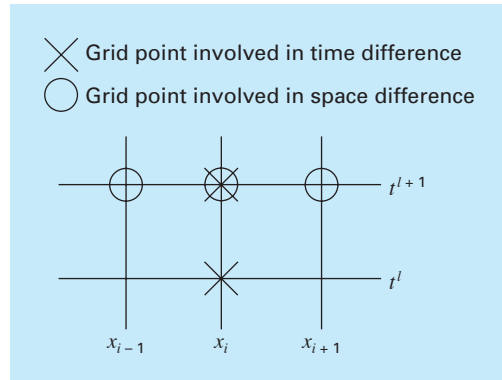
$$T_3^2 = 0.0618$$

$$T_4^2 = 1.9653$$

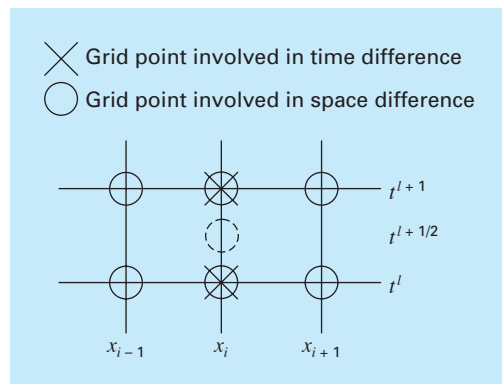
Whereas the implicit method described is stable and convergent, it has the defect that the temporal difference approximation is first-order accurate, whereas the spatial difference approximation is second-order accurate (Fig. 30.8). In the next section we present an alternative implicit method that remedies the situation.

Before proceeding, it should be mentioned that, although the simple implicit method is unconditionally stable, there is an accuracy limit to the use of large time steps. Consequently, it is not that much more efficient than the explicit approaches for most time-variable problems.

Where it does shine is for steady-state problems. Recall from Chap. 29 that a form of Gauss-Seidel (Liebmann's method) can be used to obtain steady-state solutions for elliptic equations. An alternative approach would be to run a time-variable solution until it reached a steady state. In such cases, because inaccurate intermediate results are not an issue, implicit methods allow you to employ larger time steps, and hence, can generate steady-state results in an efficient manner.

**FIGURE 30.8**

A computational molecule for the simple implicit method.

**FIGURE 30.9**

A computational molecule for the Crank-Nicolson method.

30.4 THE CRANK-NICOLSON METHOD

The *Crank-Nicolson method* provides an alternative implicit scheme that is second-order accurate in both space and time. To provide this accuracy, difference approximations are developed at the midpoint of the time increment (Fig. 30.9). To do this, the temporal first derivative can be approximated at $t^{l+1/2}$ by

$$\frac{\partial T}{\partial t} \cong \frac{T_i^{l+1} - T_i^l}{\Delta t} \quad (30.12)$$

The second derivative in space can be determined at the midpoint by averaging the difference approximations at the beginning (t^l) and at the end (t^{l+1}) of the time increment

$$\frac{\partial^2 T}{\partial x^2} \cong \frac{1}{2} \left[\frac{T_{i+1}^l - 2T_i^l + T_{i-1}^l}{(\Delta x)^2} + \frac{T_{i+1}^{l+1} - 2T_i^{l+1} + T_{i-1}^{l+1}}{(\Delta x)^2} \right] \quad (30.13)$$

Substituting Eqs. (30.12) and (30.13) into Eq. (30.1) and collecting terms gives

$$-\lambda T_{i-1}^{l+1} + 2(1+\lambda)T_i^{l+1} - \lambda T_{i+1}^{l+1} = \lambda T_{i-1}^l + 2(1-\lambda)T_i^l + \lambda T_{i+1}^l \quad (30.14)$$

where $\lambda = k \Delta t / (\Delta x)^2$. As was the case with the simple implicit approach, boundary conditions of $T_0^{l+1} = f_0(t^{l+1})$ and $T_{m+1}^{l+1} = f_{m+1}(t^{l+1})$ can be prescribed to derive versions of Eq. (30.14) for the first and the last interior nodes. For the first interior node

$$2(1+\lambda)T_1^{l+1} - \lambda T_2^{l+1} = \lambda f_0(t^l) + 2(1-\lambda)T_1^l + \lambda T_2^l + \lambda f_0(t^{l+1}) \quad (30.15)$$

and for the last interior node,

$$-\lambda T_{m-1}^{l+1} + 2(1+\lambda)T_m^{l+1} = \lambda f_{m+1}(t^l) + 2(1-\lambda)T_m^l + \lambda T_{m-1}^l + \lambda f_{m+1}(t^{l+1}) \quad (30.16)$$

Although Eqs. (30.14) through (30.16) are slightly more complicated than Eqs. (30.8), (30.10), and (30.11), they are also tridiagonal and, therefore, efficient to solve.

EXAMPLE 30.3

Crank-Nicolson Solution to the Heat-Conduction Equation

Problem Statement. Use the Crank-Nicolson method to solve the same problem as in Examples 30.1 and 30.2.

Solution. Equations (30.14) through (30.16) can be employed to generate the following tridiagonal set of equations:

$$\begin{bmatrix} 2.04175 & -0.020875 & & \\ -0.020875 & 2.04175 & -0.020875 & \\ & -0.020875 & 2.04175 & -0.020875 \\ & & -0.020875 & 2.04175 \end{bmatrix} \begin{Bmatrix} T_1^1 \\ T_2^1 \\ T_3^1 \\ T_4^1 \end{Bmatrix} = \begin{Bmatrix} 4.175 \\ 0 \\ 0 \\ 2.0875 \end{Bmatrix}$$

which can be solved for the temperatures at $t = 0.1$ s:

$$\begin{aligned} T_1^1 &= 2.0450 \\ T_2^1 &= 0.0210 \\ T_3^1 &= 0.0107 \\ T_4^1 &= 1.0225 \end{aligned}$$

To solve for the temperatures at $t = 0.2$ s, the right-hand-side vector must be changed to

$$\begin{Bmatrix} 8.1801 \\ 0.0841 \\ 0.0427 \\ 4.0901 \end{Bmatrix}$$

The simultaneous equations can then be solved for

$$\begin{aligned} T_1^2 &= 4.0073 \\ T_2^2 &= 0.0826 \\ T_3^2 &= 0.0422 \\ T_4^2 &= 2.0036 \end{aligned}$$

30.4.1 Comparison of One-Dimensional Methods

Equation (30.1) can be solved analytically. For example, a solution is available for the case where the rod's temperature is initially at zero. At $t = 0$, the boundary condition at $x = L$ is instantaneously increased to a constant level of T while $T(0)$ is held at zero. For this case, the temperature can be computed by

$$T = \bar{T} \left[\frac{x}{L} + \sum_{n=0}^{\infty} \frac{2}{n\pi} (-1)^n \sin\left(\frac{n\pi}{L}\right) \exp\left(-\frac{n^2\pi^2 k t}{L^2}\right) \right] \quad (30.17)$$

where L = total length of the rod. This equation can be employed to compute the evolution of the temperature distribution for each boundary condition. Then, the total solution can be determined by superposition.

EXAMPLE 30.4

Comparison of Analytical and Numerical Solutions

Problem Statement. Compare the analytical solution from Eq. (30.17) with numerical results obtained with the explicit, simple implicit, and Crank-Nicolson techniques. Perform the comparison for the rod employed in Examples 30.1, 30.2, and 30.3.

Solution. Recall from the previous examples that $k = 0.835 \text{ cm}^2/\text{s}$, $L = 10 \text{ cm}$, and $\Delta x = 2 \text{ cm}$. For this case, Eq. (30.17) can be used to predict that the temperature at $x = 2 \text{ cm}$, and $t = 10 \text{ s}$ would equal 64.8018. Table 30.1 presents numerical predictions of $T(2, 10)$. Notice that a range of time steps are employed. These results indicate a number of properties of the numerical methods. First, it can be seen that the explicit method is unstable for high values of λ . This instability is not manifested by either implicit approach. Second, the Crank-Nicolson method converges more rapidly as λ is decreased and provides moderately accurate results even when λ is relatively high. These outcomes are as expected because Crank-Nicolson is second-order accurate with respect to both independent variables. Finally, notice that as λ decreases, the methods seem to be converging on a value of 64.73 that is different than the analytical result of 64.80. This should not be surprising because a fixed value of $\Delta x = 2$ is used to characterize the x dimension. If both Δx and Δt were decreased as λ was decreased (that is, more spatial segments were used), the numerical solution would more closely approach the analytical result.

TABLE 30.1 Comparison of three methods of solving a parabolic PDE: the heated rod. The results shown are for temperature at $t = 10 \text{ s}$ at $x = 2 \text{ cm}$ for the rod from Examples 30.1 through 30.3. Note that the analytical solution is $T(2, 10) = 64.8018$.

Δt	λ	Explicit	Implicit	Crank-Nicolson
10	2.0875	208.75	53.01	79.77
5	1.04375	-9.13	58.49	64.79
2	0.4175	67.12	62.22	64.87
1	0.20875	65.91	63.49	64.77
0.5	0.104375	65.33	64.12	64.74
0.2	0.04175	64.97	64.49	64.73

The Crank-Nicolson method is often used for solving linear parabolic PDEs in one spatial dimension. Its advantages become even more pronounced for more complicated applications such as those involving unequally spaced meshes. Such nonuniform spacing is often advantageous where we have foreknowledge that the solution varies rapidly in local portions of the system. Further discussion of such applications and the Crank-Nicolson method in general can be found elsewhere (Ferziger, 1981; Lapidus and Pinder, 1981; Hoffman 1992).

30.5 PARABOLIC EQUATIONS IN TWO SPATIAL DIMENSIONS

The heat-conduction equation can be applied to more than one spatial dimension. For two dimensions, its form is

$$\frac{\partial T}{\partial t} = k \left(\frac{\partial^2 T}{\partial x^2} + \frac{\partial^2 T}{\partial y^2} \right) \quad (30.18)$$

One application of this equation is to model the temperature distribution on the face of a heated plate. However, rather than characterizing its steady-state distribution, as was done in Chap. 29, Eq. (30.18) provides a means to compute the plate's temperature distribution as it changes in time.

30.5.1 Standard Explicit and Implicit Schemes

An explicit solution can be obtained by substituting finite-difference approximations of the form of Eqs. (30.2) and (30.3) into Eq. (30.18). However, as with the one-dimensional case, this approach is limited by a stringent stability criterion. For the two-dimensional case, the criterion is

$$\Delta t \leq \frac{1}{8} \frac{(\Delta x)^2 + (\Delta y)^2}{k}$$

Thus, for a uniform grid ($\Delta x = \Delta y$), $\lambda = k \Delta t / (\Delta x)^2$ must be less than or equal to 1/4. Consequently, halving the step size results in a fourfold increase in the number of nodes and a 16-fold increase in computational effort.

As was the case with one-dimensional systems, implicit techniques offer alternatives that guarantee stability. However, the direct application of implicit methods such as the Crank-Nicolson technique leads to the solution of $m \times n$ simultaneous equations. Additionally, when written for two or three spatial dimensions, these equations lose the valuable property of being tridiagonal. Thus, matrix storage and computation time can become exorbitantly large. The method described in the next section offers one way around this dilemma.

30.5.2 The ADI Scheme

The alternating-direction implicit, or ADI, scheme provides a means for solving parabolic equations in two spatial dimensions using tridiagonal matrices. To do this, each time

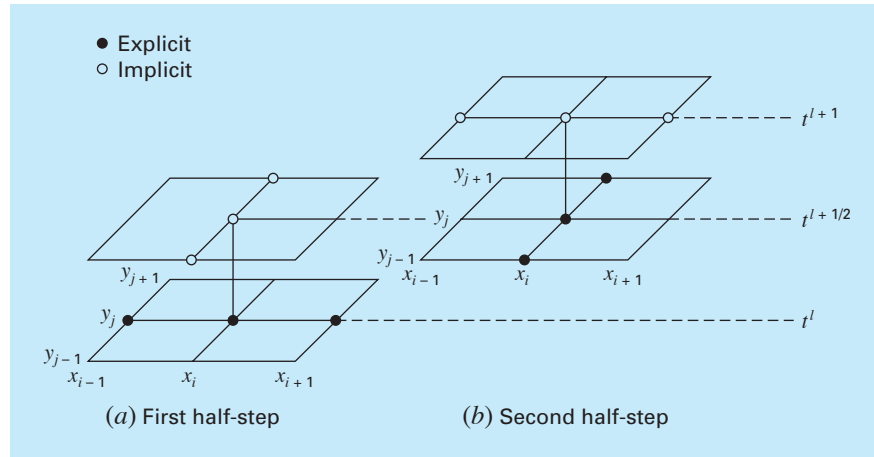


FIGURE 30.10

The two half-steps used in implementing the alternating-direction implicit scheme for solving parabolic equations in two spatial dimensions

increment is executed in two steps (Fig. 30.10). For the first step, Eq. (30.18) is approximated by

$$\frac{T_{i,j}^{l+1/2} - T_{i,j}^l}{\Delta t/2} = k \left[\frac{T_{i+1,j}^l - 2T_{i,j}^l + T_{i-1,j}^l}{(\Delta x)^2} + \frac{T_{i,j+1}^{l+1/2} - 2T_{i,j}^{l+1/2} + T_{i,j-1}^{l+1/2}}{(\Delta y)^2} \right] \quad (30.19)$$

Thus, the approximation of $\partial^2 T / \partial x^2$ is written explicitly—that is, at the base point t^l where values of temperature are known. Consequently, only the three temperature terms in the approximation of $\partial^2 T / \partial y^2$ are unknown. For the case of a square grid ($\Delta y = \Delta x$), this equation can be expressed as

$$-\lambda T_{i,j-1}^{l+1/2} + 2(1+\lambda)T_{i,j}^{l+1/2} - \lambda T_{i,j+1}^{l+1/2} = \lambda T_{i-1,j}^l + 2(1-\lambda)T_{i,j}^l + \lambda T_{i+1,j}^l \quad (30.20)$$

which, when written for the system, results in a tridiagonal set of simultaneous equations.

For the second step from $t^{l+1/2}$ to t^{l+1} , Eq. (30.18) is approximated by

$$\frac{T_{i,j}^{l+1} - T_{i,j}^{l+1/2}}{\Delta t/2} = k \left[\frac{T_{i+1,j}^{l+1} - 2T_{i,j}^{l+1} + T_{i-1,j}^{l+1}}{(\Delta x)^2} + \frac{T_{i,j+1}^{l+1/2} - 2T_{i,j}^{l+1/2} + T_{i,j-1}^{l+1/2}}{(\Delta y)^2} \right] \quad (30.21)$$

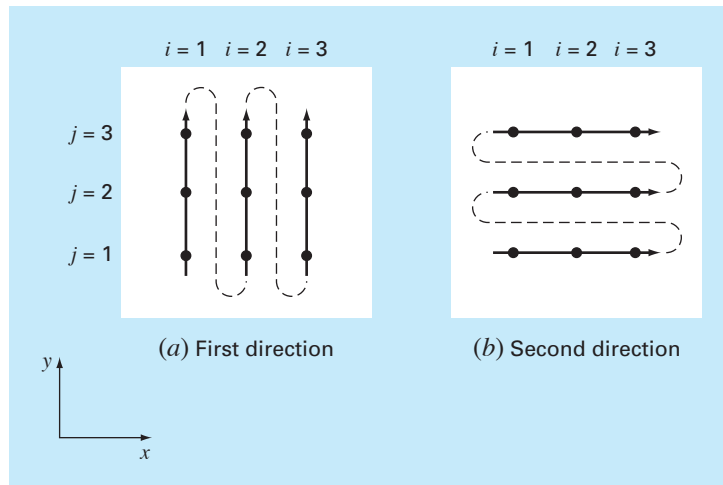
In contrast to Eq. (30.19), the approximation of $\partial^2 T / \partial x^2$ is now implicit. Thus, the bias introduced by Eq. (30.19) will be partially corrected. For a square grid, Eq. (30.21) can be written as

$$-\lambda T_{i-1,j}^{l+1} + 2(1+\lambda)T_{i,j}^{l+1} - \lambda T_{i+1,j}^{l+1} = \lambda T_{i,j-1}^{l+1/2} + 2(1-\lambda)T_{i,j}^{l+1/2} + \lambda T_{i,j+1}^{l+1/2} \quad (30.22)$$

Again, when written for a two-dimensional grid, the equation results in a tridiagonal system (Fig. 30.11). As in the following example, this leads to an efficient numerical solution.

FIGURE 30.11

The ADI method only results in tridiagonal equations if it is applied along the dimension that is implicit. Thus, on the first step (a), it is applied along the y dimension and, on the second step (b), along the x dimension. These “alternating directions” are the root of the method’s name.

**EXAMPLE 30.5****ADI Method**

Problem Statement. Use the ADI method to solve for the temperature of the plate in Examples 29.1 and 29.2. At $t = 0$, assume that the temperature of the plate is zero and the boundary temperatures are instantaneously brought to the levels shown in Fig. 29.4. Employ a time step of 10 s. Recall from Example 30.1 that the coefficient of thermal diffusivity for aluminum is $k = 0.835 \text{ cm}^2/\text{s}$.

Solution. A value of $\Delta x = 10 \text{ cm}$ was employed to characterize the $40 \times 40\text{-cm}$ plate from Examples 29.1 and 29.2. Therefore, $\lambda = 0.835(10)/(10)^2 = 0.0835$. For the first step to $t = 5$ (Fig. 30.11a), Eq. (30.20) is applied to nodes (1, 1), (1, 2), and (1, 3) to yield the following tridiagonal equations:

$$\begin{bmatrix} 2.167 & -0.0835 & 0 \\ -0.0835 & 2.167 & -0.0835 \\ 0 & -0.0835 & 2.167 \end{bmatrix} \begin{Bmatrix} T_{1,1} \\ T_{1,2} \\ T_{1,3} \end{Bmatrix} = \begin{Bmatrix} 6.2625 \\ 6.2625 \\ 14.6125 \end{Bmatrix}$$

which can be solved for

$$T_{1,1} = 3.01597 \quad T_{1,2} = 3.2708 \quad T_{1,3} = 6.8692$$

In a similar fashion, tridiagonal equations can be developed and solved for

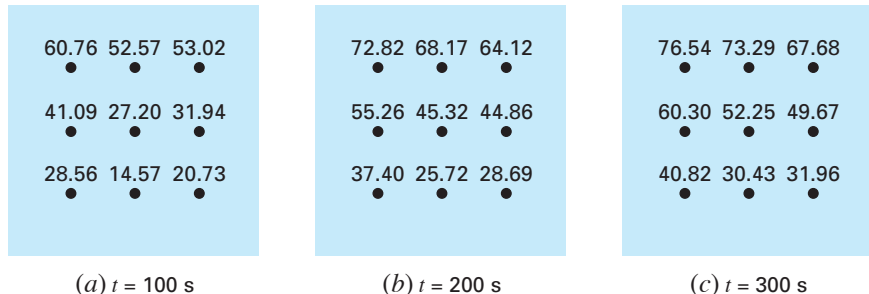
$$T_{2,1} = 0.1274 \quad T_{2,2} = 0.2900 \quad T_{2,3} = 4.1291$$

and

$$T_{3,1} = 2.0181 \quad T_{3,2} = 2.2477 \quad T_{3,3} = 6.0256$$

For the second step to $t = 10$ (Fig. 30.11b), Eq. (30.22) is applied to nodes (1, 1), (2, 1), and (3, 1) to yield

$$\begin{bmatrix} 2.167 & -0.0835 & 0 \\ -0.0835 & 2.167 & -0.0835 \\ 0 & -0.0835 & 2.167 \end{bmatrix} \begin{Bmatrix} T_{1,1} \\ T_{2,1} \\ T_{3,1} \end{Bmatrix} = \begin{Bmatrix} 12.0639 \\ 0.2577 \\ 8.0619 \end{Bmatrix}$$

(a) $t = 100$ s(b) $t = 200$ s(c) $t = 300$ s**FIGURE 30.12**

Solution for the heated plate from Example 30.5 at (a) $t = 100$ s, (b) $t = 200$ s, and (c) $t = 300$ s.

which can be solved for

$$T_{1,1} = 5.5855 \quad T_{2,1} = 0.4782 \quad T_{3,1} = 3.7388$$

Tridiagonal equations for the other rows can be developed and solved for

$$T_{1,2} = 6.1683 \quad T_{2,2} = 0.8238 \quad T_{3,2} = 4.2359$$

and

$$T_{1,3} = 13.1120 \quad T_{2,3} = 8.3207 \quad T_{3,3} = 11.3606$$

The computation can be repeated, and the results for $t = 100$, 200, and 300 s are depicted in Fig. 30.12a through c, respectively. As expected, the temperature of the plate rises. After a sufficient time elapses, the temperature will approach the steady-state distribution of Fig. 29.5.

The ADI method is but one of a group of techniques called splitting methods. Some of these represent efforts to circumvent shortcomings of ADI. Discussion of other splitting methods as well as more information on ADI can be found elsewhere (Ferziger, 1981; Lapidus and Pinder, 1981).

PROBLEMS

30.1 Repeat Example 30.1, but use the midpoint method to generate your solution.

30.2 Repeat Example 30.1, but for the case where the rod is initially at 50°C and the derivative at $x = 0$ is equal to 1 and at $x = 10$ is equal to 0. Interpret your results.

30.3 (a) Repeat Example 30.1, but for a time step of $\Delta t = 0.05$ s. Compute results to $t = 0.2$. **(b)** In addition, perform the same computation with the Heun method (without iteration of the corrector)

with a much smaller step size of $\Delta t = 0.001$ s. Assuming that the results of (b) are a valid approximation of the true solution, determine percent relative errors for the results obtained in Example 30.1 as well as for part (a).

30.4 Repeat Example 30.2, but for the case where the derivative at $x = 10$ is equal to zero.

30.5 Repeat Example 30.3, but for $\Delta x = 1$ cm.

30.6 Repeat Example 30.5, but for the plate described in Prob. 29.2.

30.7 The advection-diffusion equation is used to compute the distribution of concentration along the length of a rectangular chemical reactor (see Sec. 32.1),

$$\frac{\partial c}{\partial t} = D \frac{\partial^2 c}{\partial x^2} - U \frac{\partial c}{\partial x} - kc$$

where c = concentration (mg/m^3), t = time (min), D = a diffusion coefficient (m^2/min), x = distance along the tank's longitudinal axis (m) where $x = 0$ at the tank's inlet, U = velocity in the x direction (m/min), and k = a reaction rate (min^{-1}) whereby the chemical decays to another form. Develop an explicit scheme to solve this equation numerically. Test it for $k = 0.15$, $D = 100$, and $U = 1$ for a tank of length 10 m. Use a $\Delta x = 1$ m, and a step size $\Delta t = 0.005$. Assume that the inflow concentration is 100 and that the initial concentration in the tank is zero. Perform the simulation from $t = 0$ to 100 and plot the final resulting concentrations versus x .

30.8 Develop a user-friendly computer program for the simple explicit method from Sec. 30.2. Test it by duplicating Example 30.1.

30.9 Modify the program in Prob. 30.8 so that it employs either Dirichlet or derivative boundary conditions. Test it by solving Prob. 30.2.

30.10 Develop a user-friendly computer program to implement the simple implicit scheme from Sec. 30.3. Test it by duplicating Example 30.2.

30.11 Develop a user-friendly computer program to implement the Crank-Nicolson method from Sec. 30.4. Test it by duplicating Example 30.3.

30.12 Develop a user-friendly computer program for the ADI method described in Sec. 30.5. Test it by duplicating Example 30.5.

30.13 The nondimensional form for the transient heat conduction in an insulated rod (Eq. 30.1) can be written as

$$\frac{\partial^2 u}{\partial \bar{x}^2} = \frac{\partial u}{\partial \bar{t}}$$

where nondimensional space, time, and temperature are defined as

$$\bar{x} = \frac{x}{L} \quad \bar{t} = \frac{T}{(\rho CL^2/k)} \quad u = \frac{T - T_o}{T_L - T_o}$$

where L = the rod length, k = thermal conductivity of the rod material, ρ = density, C = specific heat, T_o = temperature at $x = 0$, and T_L = temperature at $x = L$. This makes for the following boundary and initial conditions:

Boundary conditions	$u(0, \bar{t}) = 0$	$u(1, \bar{t}) = 0$
Initial conditions	$u(\bar{x}, 0) = 0$	$0 \leq \bar{x} \leq 1$

Solve this nondimensional equation for the temperature distribution using finite-difference methods and a second-order accurate Crank-Nicolson formulation to integrate in time. Write a computer program to obtain the solution. Increase the value of $\Delta \bar{t}$ by 10% for

each time step to more quickly obtain the steady-state solution, and select values of $\Delta \bar{x}$ and $\Delta \bar{t}$ for good accuracy. Plot the nondimensional temperature versus nondimensional length for various values of nondimensional times.

30.14 The problem of transient radial heat flow in a circular rod in nondimensional form is described by

$$\frac{\partial^2 u}{\partial \bar{r}^2} + \frac{1}{\bar{r}} \frac{\partial u}{\partial \bar{r}} = \frac{\partial u}{\partial \bar{t}}$$

Boundary conditions	$u(1, \bar{t}) = 1$	$\frac{\partial u}{\partial \bar{r}}(0, \bar{t}) = 0$
Initial conditions	$u(\bar{x}, 0) = 0$	$0 \leq \bar{x} \leq 1$

Solve the nondimensional transient radial heat-conduction equation in a circular rod for the temperature distribution at various times as the rod temperature approaches steady state. Use second-order accurate finite-difference analogues for the derivatives with a Crank-Nicolson formulation. Write a computer program for the solution. Select values of $\Delta \bar{r}$ and $\Delta \bar{t}$ for good accuracy. Plot the temperature u versus radius \bar{r} for various times \bar{t} .

30.15 Solve the following PDE:

$$\frac{\partial^2 u}{\partial x^2} + b \frac{\partial u}{\partial x} = \frac{\partial u}{\partial t}$$

Boundary conditions	$u(0, t) = 0$	$u(1, t) = 0$
Initial conditions	$u(x, 0) = 0$	$0 \leq x \leq 1$

Use second-order accurate finite-difference analogues for the derivatives with a Crank-Nicolson formulation to integrate in time. Write a computer program for the solution. Increase the value of Δt by 10% for each time step to more quickly obtain the steady-state solution, and select values of Δx and Δt for good accuracy. Plot u versus x for various values of t . Solve for values of $b = 4, 2, 0, -2, -4$.

30.16 Determine the temperatures along a 1-m horizontal rod described by the heat-conduction equation (Eq. 30.1). Assume that the right boundary is insulated and that the left boundary ($x = 0$) is represented by

$$-k' \frac{\partial T}{\partial x} \Big|_{x=0} = h(T_a - T_0)$$

where k' = coefficient of thermal conductivity ($\text{W/m} \cdot ^\circ\text{C}$), h = convective heat transfer coefficient ($\text{W/m}^2 \cdot ^\circ\text{C}$), T_a = ambient temperature ($^\circ\text{C}$), and T_0 = temperature of the rod at $x = 0$ ($^\circ\text{C}$). Solve for temperature as a function of time using a spatial step of $\Delta x = 1$ cm and the following parameter values: $k = 2 \times 10^{-5} \text{ m}^2/\text{s}$, $k' = 10 \text{ W/m} \cdot ^\circ\text{C}$, $h = 25 \text{ W/m}^2 \cdot ^\circ\text{C}$, and $T_a = 50^\circ\text{C}$. Assume that the initial temperature of the rod is zero.